Preliminary Back Analysis of Open Hillside Landslide Impacting on a Flexible Rockfall Barrier at Jordan Valley

GEO Report No. 308

J.S.H. Kwan & R.C.H. Koo

Geotechnical Engineering Office
Civil Engineering and Development Department
The Government of the Hong Kong Special Administrative Region

Preliminary Back Analysis of Open Hillside Landslide Impacting on a Flexible Rockfall Barrier at Jordan Valley

GEO Report No. 308

J.S.H. Kwan & R.C.H. Koo

This report was originally produced in January 2013 as GEO Special Project Report No. SPR 1/2013

Table of Contents
Table of Contents
Table of Contents
Table of Contents

First published, April 2015

Prepared by:

Geotechnical Engineering Office,
Civil Engineering and Development Department,
Civil Engineering and Development Building,
101 Princess Margaret Road,
Homantin, Kowloon,
Hong Kong.

Table of Contents
Table of Contents
Table of Contents
Table of Contents

Preface

In keeping with our policy of releasing information which may be of general interest to the geotechnical profession and the public, we make available selected internal reports in a series of publications termed the GEO Report series. The GEO Reports can be downloaded from the website of the Civil Engineering and Development Department (http://www.cedd.gov.hk) on the Internet. Printed copies are also available for some GEO Reports. For printed copies, a charge is made to cover the cost of printing.

The Geotechnical Engineering Office also produces documents specifically for publication in print. These include guidance documents and results of comprehensive reviews. They can also be downloaded from the above website.

The publications and the printed GEO Reports may be obtained from the Government's Information Services Department. Information on how to purchase these documents is given on the second last page of this report.

H.N. Wong
Head, Geotechnical Engineering Office
April 2015

Table of Contents
Table of Contents
Table of Contents
Table of Contents

Foreword

This report presents the results of a study of an open hillside failure impacting on a flexible rockfall barrier at Jordan Valley, Hong Kong. This study was carried out by Dr J.S.H. Kwan and Mr R.C.H. Koo under my supervision. It comprised an investigation of the mobility of the open hillside failure and structural analyses of the flexible rockfall barrier which was impacted by the landslide debris. Mr T.H. Lo assisted in the structural analyses. Computer program NIDA-MNN developed by the Hong Kong Polytechnic University was adopted in the structural analysis.

Draft versions of the report were reviewed by Professor S.L. Chan of the Hong Kong Polytechnic University, Dr Benoit Boutillier of Heaven Climber and Dr J.C.Y. Cheuk of AECOM. Professor S.L. Chan is the developer of the computer program NIDA-MNN. Dr Benoit Boutillier is the engineer of the manufacturer of the flexible rockfall barrier. Dr J.C.Y. Cheuk is the Landslip Investigation Consultants who carried out the post-landslide inspection. Dr A.K.T. Chong of AECOM also provided useful comments on the structural analysis. Contributions from all parties are gratefully acknowledged.

Y.K. Shiu
Chief Geotechnical Engineer/Standards & Testing

Abstract

Debris from an open hillside landslide struck flexible rockfall barrier no. 11NE-A/ND8 at Jordan Valley, Hong Kong, in 2008. The landslide was sourced from a natural hillside. The landslide scar is 10 m wide and 7 m long, and the landslide volume is about 110 m^3. The rockfall barrier was originally designed to mitigate boulder fall at the site location. The landslide debris was largely retained by the barrier but two of the barrier posts were severely damaged and failed. This is so far the only case history of landslide debris having been intercepted by flexible barrier in Hong Kong.

Back analyses of this case history have been undertaken with a view to obtaining a better understanding of the behaviour of flexible debris-resisting barriers upon debris impact. Numerical simulations of mobility of the landslide debris and structural response of the flexible barrier have been carried out, which reproduce some of the salient field observations. Possible contributory factors to the failure of the posts and insights established from the back analyses are documented in this report.

Table of Contents
Table of Contents
Table of Contents
Table of Contents

Contents

List of Tables

Table of Contents
Table of Contents
Table of Contents

List of Figures

Table of Contents
Table of Contents
Table of Contents

1 Introduction

An open hillside landslide in Jordan Valley was reported to the GEO in December 2009. A subsequent aerial photograph interpretation study by the Landslip Investigation Consultants (LIC) suggested that the landslide could have occurred during a heavy rainstorm in June 2008. Ground mass of about 110 m^3 in volume detached from a natural hillside in the form of an open hillside failure. The landslide debris struck flexible rockfall barrier no. 11NE-A/ND8 near the toe of the hillside. So far, this is the only case history of flexible barrier intercepting landslide debris in Hong Kong. Preliminary back analyses of this case history have been carried out with a view to obtaining insights that are pertinent to the design of flexible debris-resisting barriers.

2 The Landslide and Flexible Rockfall Barrier

The locations of the landslide site and flexible rockfall barrier no. 11NE-A/ND8 are shown in Figure 2.1. The flexible rockfall barrier was originally designed to mitigate boulder fall hazard from the natural hillside (LMM, 2004). The height of the steel posts is 5 m but the minimum height of the ring nets is 4 m and its designed energy capacity is 1,000 kJ. Posts of the barrier are at 10 m spacing and supported on concrete pad footings of 400 mm by 400 mm in dimensions. The embedment depth of the footings is about 500 mm. Barrier posts are made of 140 mm by 140 mm steel hollow section, with a steel thickness of 4 mm.

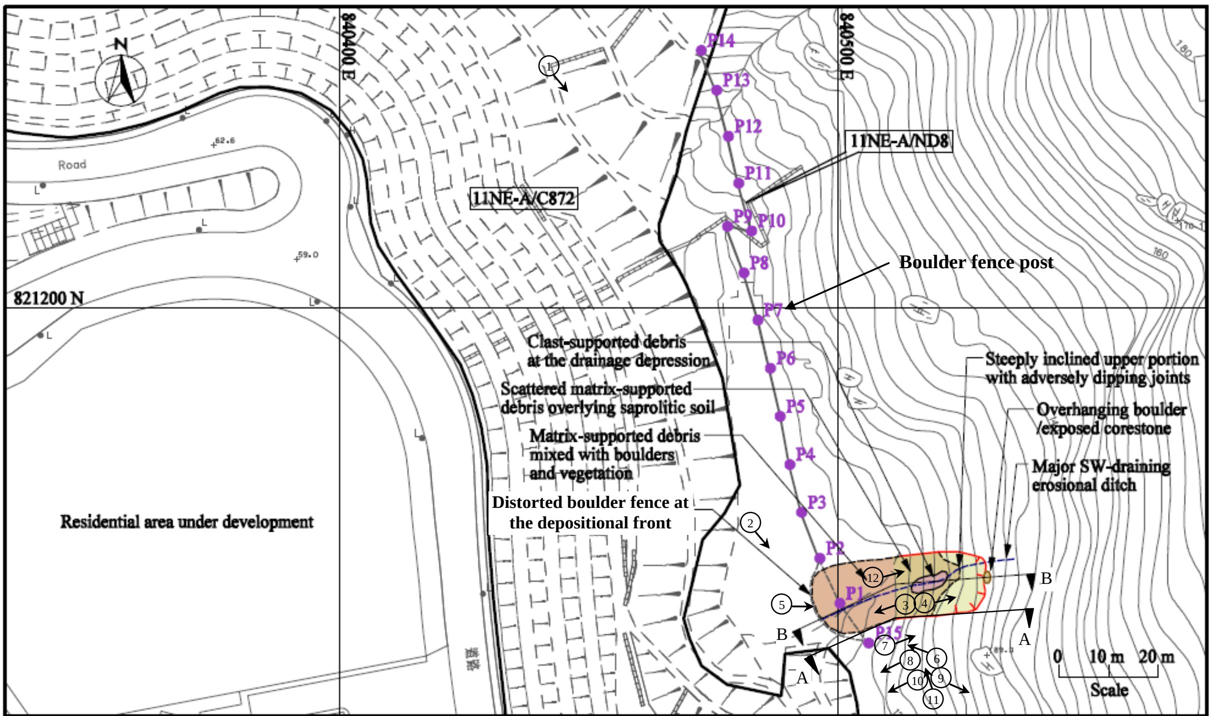

Note : Base plan is extracted from 1 : 1000 survey sheets Nos. 11NE-12B, 11NE-12D, 11NE-13A and 11NE-13C dated July 2009.

Figure 2.1 Locations of the Landslide Site and Flexible Rockfall Barrier No. 11NE-A/ND8

Table of Contents
Table of Contents
Table of Contents
Table of Contents

Site inspections by the LIC were carried out in December 2009 and April 2010. The Standards & Testing Division joined the inspection in April 2010. It was observed that landslide debris struck Post P1 and two ring net panels spanning across Posts P2-P1 and Posts P1-P15 (see Figure 2.1). The debris was largely retained by the barrier. There were no noticeable signs of overflow or marks left behind by a large amount of debris passing through the ring net. Close inspection of the ring net indicated that landslide debris, including fine grains, was arrested by the barrier (see Figure 2.2). Post P1 was severely damaged by debris impact. No signs of damage to Post P2 were evident. Post P15, which was located at the southern end of the barrier, was not subject to any direct impact by the landslide debris. However, Post P15 had bent and failed. It was also observed during the inspections that the energy dissipation devices attached to the uphill cable ropes of the barrier had not been mobilised, and no tensile failure of any cable ropes was apparent. Details of the site observations are presented in an inspection note prepared by the LIC. The inspection note is reproduced in Appendix A.

It is noteworthy that the construction details of Post P15 are different from the intermediate Posts P1 and P2. The ring net was attached to Post P15 by about nine layers of stainless steel bands (see Figure 2.3), whereas Posts P1 and P2 were not tied to any ring net (see Figure 2.4).

Figure 2.2 Close Inspection to the Ring Net

Table of Contents
Table of Contents
Table of Contents
Table of Contents

Figure 2.3 Photograph of Post P15 **Figure 2.4 Photograph of Post P2**

The salient observations made by the LIC are summarised below:

(a) two barrier posts (P1 and P15) were severely deformed and failed,

(b) Post P15 did not exhibit any signs of direct impact by debris but it had bent,

(c) the two posts P1 and P15, together with their concrete footings, were found to have displaced forward by about 1 to 2 m,

(d) energy dissipation devices attached to the uphill extension cable ropes of the barrier had not been mobilised (see Appendix A), and

(e) no tensile failure of any cable ropes was apparent.

3 Mobility of Landslide Debris

Figure 3.1 shows a cross-section (Section B-B of Figure 2.1) along the centerline of the landslide debris trail. The travel angle of the landslide debris, accounting for the retarding effect of the flexible barrier, is about 27°. This travel angle does not represent the

Table of Contents
Table of Contents
Table of Contents
Table of Contents

true mobility of the landslide debris because the debris was obstructed by the flexible barrier. If the frictional rheology is adopted to back analyse the landslide mobility, an apparent basal friction angle (ϕ) of less than 27° should be used. GEO (2012) presents a review of the mobility of open hillside failures, which shows that the lower bound value of ϕ for open hillside failures in Hong Kong is 25° for landslide volume less than 500 m^3. It is therefore assumed that the ϕ value of this Jordan Valley landslide could be around 25° to 26°, and a ϕ value of 25° has been adopted in the back analysis. Computer program 2d-DMM (Kwan & Sun, 2006) was used for the analysis. Table 3.1 shows the debris velocity hydrograph and the debris thickness hydrograph at the original barrier location based on the 2d-DMM analyses.

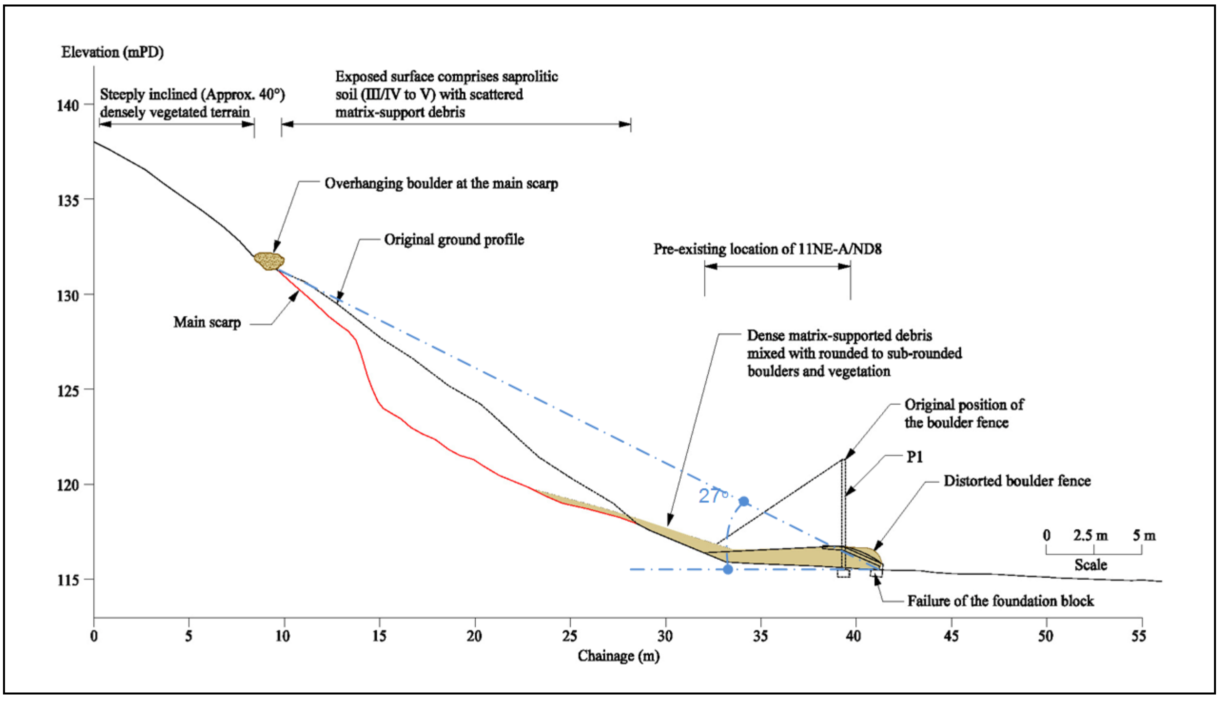

Figure 3.1 Cross-section of the Landslide Debris Trail

According to the results of the 2d-DMM analyses, the maximum frontal debris velocity at the location of the flexible barrier was about 4 m/s. After the peak value, the velocity drops to zero within 2 seconds. The calculated maximum debris thickness is about 1.2 m, which is generally consistent with the site observations.

Debris mobility analysis has been carried out without consideration of the obstruction by the barrier. However, the analysis results can shed some light on how the landslide debris could behave upon interception by the barrier. According to the debris velocity hydrograph and debris thickness hydrograph, the debris velocity could have dropped rapidly and the debris could be as thick as about 1 m. It is unlikely that the rear portion of debris mass over-rode on the frontal portion to result in multiple impacts to the barrier. This is consistent with the LIC's site observation that the landslide debris slid down the slope as a lumped mass and no evidence of multiple surge impact on the barrier was noted.

Table of Contents
Table of Contents
Table of Contents
Table of Contents

Table 3.1 Results of Debris Mobility Assessment

Debris Velocity Hydrograph at Original Barrier Location	Debris Thickness Hydrograph at Original Barrier Location
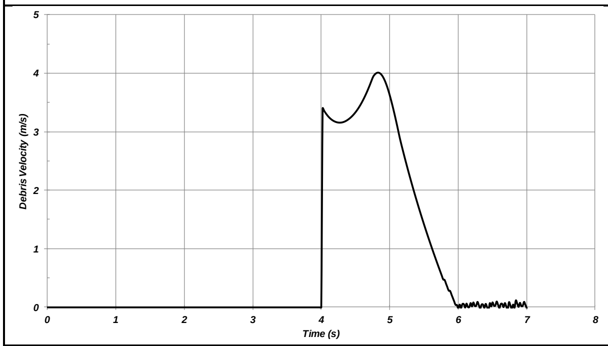	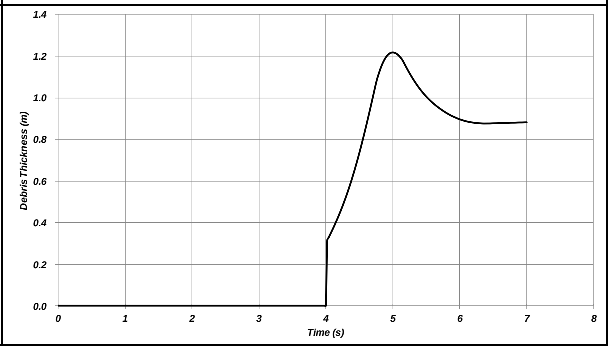

4 Energy Loading

The theoretical kinetic energy (*KE*) of landslide debris that travelled beyond the original barrier location can be estimated by coupling together the debris velocity hydrograph and debris thickness hydrograph using the following equation:

$$KE = \sum_t \frac{1}{2}[v(t)h(t)w\rho\Delta t][v(t)]^2 \quad \text{.....................................} \quad (4.1)$$

where
- $v(t)$ = debris velocity at barrier location at time t (m/s)
- $h(t)$ = debris thickness at barrier location at time t (m)
- w = debris width at barrier location, assumed to be constant
- ρ = debris density (in kg/m^3)
- Δt = observation time interval (s).

According to the site inspection, debris width (w) is about 10 m. Debris density is assumed to be 2,000 kg/m^3. With the velocity and debris hydrographs produced by the debris mobility analysis, the kinetic energy of the debris is estimated to be 463 kJ using Equation 4.1. The calculation of kinetic energy (*KE*) using Equation 4.1 does not consider the obstruction effect of the barrier and it corresponds to the *KE* at an "uninterrupted" state. In theory, this is the maximum energy loading that could be applied on the barrier.

The energy loading has also been estimated using the analytical solution developed by Sun & Law (2012). Back analyses of landslide mobility presented in Section 3 indicate that the thickness of the impacting front of the landslide debris could be in the order of 1 m. Debris frontal velocity estimated by the 2d-DMM analysis is also used in the calculation. Values of other parameters assumed for the calculation of the energy loading are listed below:

debris density:	2,000 kg/m^3
debris width:	10 m
ground inclination behind barrier:	0°
angle of ramp in run up mechanism:	10°

Table of Contents
Table of Contents
Table of Contents
Table of Contents

Sun & Law (op cit)'s analytical solution requires input of the dynamic pressure coefficient (α). The energy loadings corresponding to α = 1 and 2 respectively are calculated. The results are presented in Table 4.1.

Table 4.1 Energy Loading Calculated Based on Pile-up Mechanism and Run-up Mechanism

Pile-up Mechanism (kJ)		Run-up Mechanism (kJ)	
$\alpha = 1$	$\alpha = 2$	$\alpha = 1$	$\alpha = 2$
280	560	8	8

Since the landslide mass slid down the hillside as a lumped mass, the pile-up and run-up mechanisms assumed in the analytical solutions developed by Sun & Law (2012) may not describe the debris deposition mechanism of this case history very well. The calculated energy loadings associated with the two mechanisms are presented in this report for completeness.

5 Structural Analysis

Field observations indicated that the landslide debris was largely retained by the flexible rockfall barrier. However, it was found that Post P1 was severely deformed and had failed (see Plate 5 in Appendix A). End Post P15 was also damaged, although there was no signs of direct debris impact on this post (see Figure 3 and Plate 6 in Appendix A). It is worthwhile to examine the possible structural behaviour of the flexible barrier subject to debris impact in this landslide, which may shed some light on the possible failure mechanism of the barrier posts.

A preliminary numerical structural analysis has been carried out. The debris impact load is modelled as a pseudo-static uniformly distributed pressure (UDP) acting orthogonally on the barrier. Site observation suggests that landslide debris could have impacted on Post P1 and the netting on the two sides of the post. The results of the mobility analysis presented in Section 3 indicate that the thickness of the impact front could be in the order of 1 m. In light of this, the loaded area of UDP against the netting and Post P1 is assumed to be 1 m high. The width of the UDP is taken as 10 m, which is the observed width of the landslide. The loaded area of UDP is centered at Post P1 to tally with the site inspection. A single impact is considered in the back analysis, since no evidence of multiple surge impacts was noted on site (see also Section 3 and Appendix A).

A non-linear finite element program NIDA-MNN (Version 8.0) developed by the Hong Kong Polytechnic University is used in this study (Chan el at, 2012). This program was benchmarked by Chan et al (op cit) against Geobrugg's instrumented field data. The structural model of the flexible barrier, including an assembly of ring nets, steel posts, energy dissipating devices, rope cables, etc., has been set up in NIDA-MNN for assessing the barrier's structural response to the applied pseudo-static UDP.

The flexible barrier hit by the landslide debris is a proprietary rockfall fence with an

Table of Contents
Table of Contents
Table of Contents
Table of Contents

energy capacity of 1,000 kJ. As-built drawings were retrieved from the project file by the LIC (see Appendix A). The drawings provide information on the physical dimensions of different structural components of the barrier for setting up the numerical model in NIDA-MNN. Contact with the manufacturer of the rockfall fence had also been made to confirm the structural properties of different components of the barrier (e.g. ultimate yield strength of cable ropes, etc.) to facilitate the back analysis. Details are presented in Appendix B.

Different magnitudes of UDP are used in the analysis with an aim to replicating the observations numerically. Results show that both Posts P1 and P15 could fail by buckling when the applied UDP was increased to 50 kPa. According to the NIDA-MNN analysis, the large bending moment of P1 could result from the direct impact of landslide debris. For P15, analysis shows that the post is subject to bending moment and shear forces induced by load transferred from the ring net attached to the post. P15 probably experienced an axial compression load larger than that in P1. This larger compression load could be due to the downward forces brought about by the uphill and inclined anchor cables attached to the top of the post, as well as the deformed ring net that is connected to the post. Structural calculations (see Section B.5) show that the combined actions of bending, shear and compression could result in a buckling failure of the post. This is a possible failure mechanism of P1 and P15. In addition, the calculated base shear forces of P1 and P15 exceed the estimated sliding resistance of the footings of the posts. This agrees with the site observations that the corresponding footings had displaced from their original locations.

NIDA-MNN analysis assuming magnitudes of UDP higher than 50 kPa has also been carried out. When UDP is increased to 66 kPa, the lower rope cable would be stressed to a level that exceeds the ultimate tensile capacity (270 kN) of the cable as advised by the barrier manufacturer. Therefore, analysis based on UDP of magnitude exceeding 66 kPa has not been undertaken. For this range of UDP (i.e. 50 kPa to 66 kPa), the calculated forces, including the base shear force, of Post P2 are not large, and structural failure or foundation failure of P2 is not likely, which is consistent with the site observation.

The UDP magnitudes of 50 kPa to 66 kPa correspond to a dynamic pressure coefficient (α) of 1.6 to 2.1 ($p = \alpha \rho v^2$; p = debris impact pressure, α = dynamic pressure coefficient, ρ = debris density, and v = debris impact velocity), where ρ is assumed to be 2,000 kg/m^3 and v is assumed to be 4 m/s.

The above preliminary analyses are by no means definitive. They are only intended to shed some light on the potential order of magnitude of the operational α values. It should be emphasised that various assumptions (e.g. dimensions of the impacting debris front, orthogonal debris impact to the barrier, a constant and uniform impact pressure, fixed post base, etc.) have been adopted in the back analyses. It should be noted that since the barrier was close to the landslide initiation zone, the associated basal friction angle of the landslide debris could have been lower than that assumed in the mobility analysis[1]. If that were the case, then the debris impact velocity could have been underestimated.

---

[1] The present mobility analysis adopts a basal friction angle of 25°, which was obtained by back analyses of selected Enhanced Natural Terrain Landslide Inventory (ENTLI) cases (see also GEO TGN No. 34). This angle corresponds to the average basal friction angle over the landslide transportation process of the relevant ENTLI cases. In theory, basal friction angle of landslide debris could vary along the runout trail, and within the landslide initiation zone, the basal friction angle could be smaller as compared with the average value.

Table of Contents
Table of Contents
Table of Contents
Table of Contents

To investigate the critical load transfer between netting and post, an additional numerical analysis which does not consider the attachment of the netting to Post P15 is carried out. Results of the additional analysis show that while there is no significant change in bending moment (M_x) of Post 1, bending moment (M_y) experienced by Post P15 could be significantly reduced by 95% at UDP of 66 kPa, and no buckling failure of Post 15 could have been resulted in. It is concluded that the effect of load transfer from the netting attached on the post could be critical and should be carefully considered in the design.

The calculated base horizontal reaction in *y*-direction of Post P1 is in the order of 350 kN to 450 kN for the range of UDP (i.e. 50 kPa to 66 kPa) considered in this study. It is very likely that this reaction force has exceeded the sliding resistance of the shallow footings of the posts. As such, the corresponding footings displaced from their original locations as observed but this was not modeled in the analysis. Toe failure of P15 is also observed on site and this is probably due to lateral deformation of the netting attached to the post. However, the post-failure mechanism is not modelled by the present analysis, since a pin connection at the base of the posts is assumed.

Furthermore, the analyses are subject to the following limitations: (i) the simulations do not consider the post-failure mechanism of the structural system, such as redistribution of loads among the structural elements of the barrier system and the possibility of progressive failure, and (ii) the weight of debris retained in the bulged portion of the ring nets is neglected. The results of the present analyses infer both foundation failure and bending/buckling failure of the posts, however, the actual sequence of failure cannot be determined. In theory, once a post fails, it would shed its load to the adjacent posts through the structural elements (e.g. rope cables). Hence, the loading in the barrier system will be redistributed. It may lead to a progressive collapse until no further elements fail. However, the computer program does not consider load redistribution and hence the sequence of failure. In spite of these limitations, the preliminary back analyses could provide a basis for sensitivity analysis to give a feel of the possible load transfer mechanism of a flexible barrier upon debris impact.

6 Discussion

Some interesting observations pertaining to the possible structural behaviour of a flexible barrier that can be derived from the preliminary back analyses are summaried below:

(a) the combined action of axial force and bending moment induced by debris impact and the downward force of uphill anchor ropes and lateral anchor ropes could be critical to the post design;

(b) the location of debris impact load on barrier should be carefully chosen for design check, as in some cases, loading acting on the end panel of the barrier could represent one of the critical loading cases for design of the end posts;

(c) detailing, especially connections of structural elements, should be duly considered in the structural assessment of

Table of Contents

Table of Contents

Table of Contents

Table of Contents

flexible barrier;

(d) the need for checking the structural performance of barrier posts and brake elements that are not directly hit by landslide debris should not be overlooked;

(e) the foundations of barrier posts should be properly designed to guard against possible failure due to debris impact on the barrier; attention should be paid to the post connecting to lateral anchor, since displacement of the post may result in bending moment and shear forces on the lateral anchor (see also Figure 6.2); and

(f) due attention should be paid to proper detailing in order to ensure the mobilisation of the brake elements as per the design intent.

Site inspections revealed that brake elements attached to the uphill anchor cables were not activated and hence item (f) above is pertinent. Based on the details shown on as-built records (see Fig. X6.3 and Fig. X6.4 on Drawing no. P-010/AS/02 in Appendix A), the cables were threaded through small holes (120 mm in diameter) in the barrier posts and were connected to the top and bottom ropes. Activation of the brake elements would have required adequate extension of the uphill cables before failure of the posts. According to LMM (2004), the uphill cables are supposed to slide through the holes in the posts, in order to create sufficient cable extensions so as to mobilise the brake elements (see Figure 6.1). However, it was observed that movement of the cables could have been restrained by the friction between the cable and the post. This might be one of the factors that led to the observed non-performance of the brake elements. Apart from this, there could be other possible contributory factors. The brake elements of the flexible barrier were positioned close to the ground surface and as such, they might have been buried by the landslide debris before or when the barrier was struck, which could impede the mobilisation of the brake elements (see Plates 10 and 11 of Appendix A). Displacement and deformation of the posts resulting in structural failure and foundation failure could also have played a role in this regard, as these could affect the movement of the cable through the hole in the post.

It may be beneficial in terms of design robustness if the post foundation be able to dissipate energy during the impact. However, the energy dissipation would be associated with a certain amount of deformations or movements, which calls for repairing works afterwards. The repairing work for foundation is difficult and the performance of foundation involving deformations or movements is not easy to ascertain.

With reference to item (e) regarding failure of post foundation, it is noteworthy that the foundation of Post P15 was displaced along the direction of debris impact by about 1 m. This displacement direction is perpendicular to the lateral cable, which resulted in bending actions on the ground anchor of the lateral cable. This probably caused the damage in the grout core of the anchor as observed on site (see Figure 6.2). Therefore, displacement of the posts, depending on the direction of the displacement, could have implications on anchor foundations of the lateral cables.

Table of Contents
Table of Contents
Table of Contents
Table of Contents

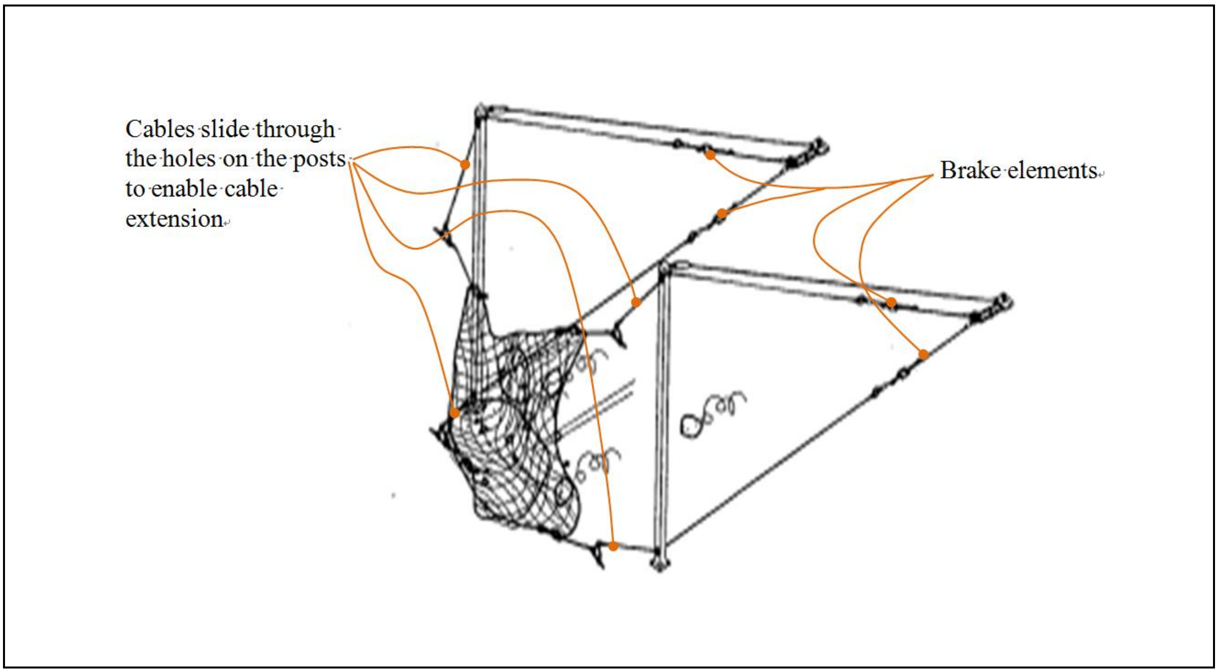

Figure 6.1 Activation of Brake Elements and Extension of Cables (LMM, 2004)

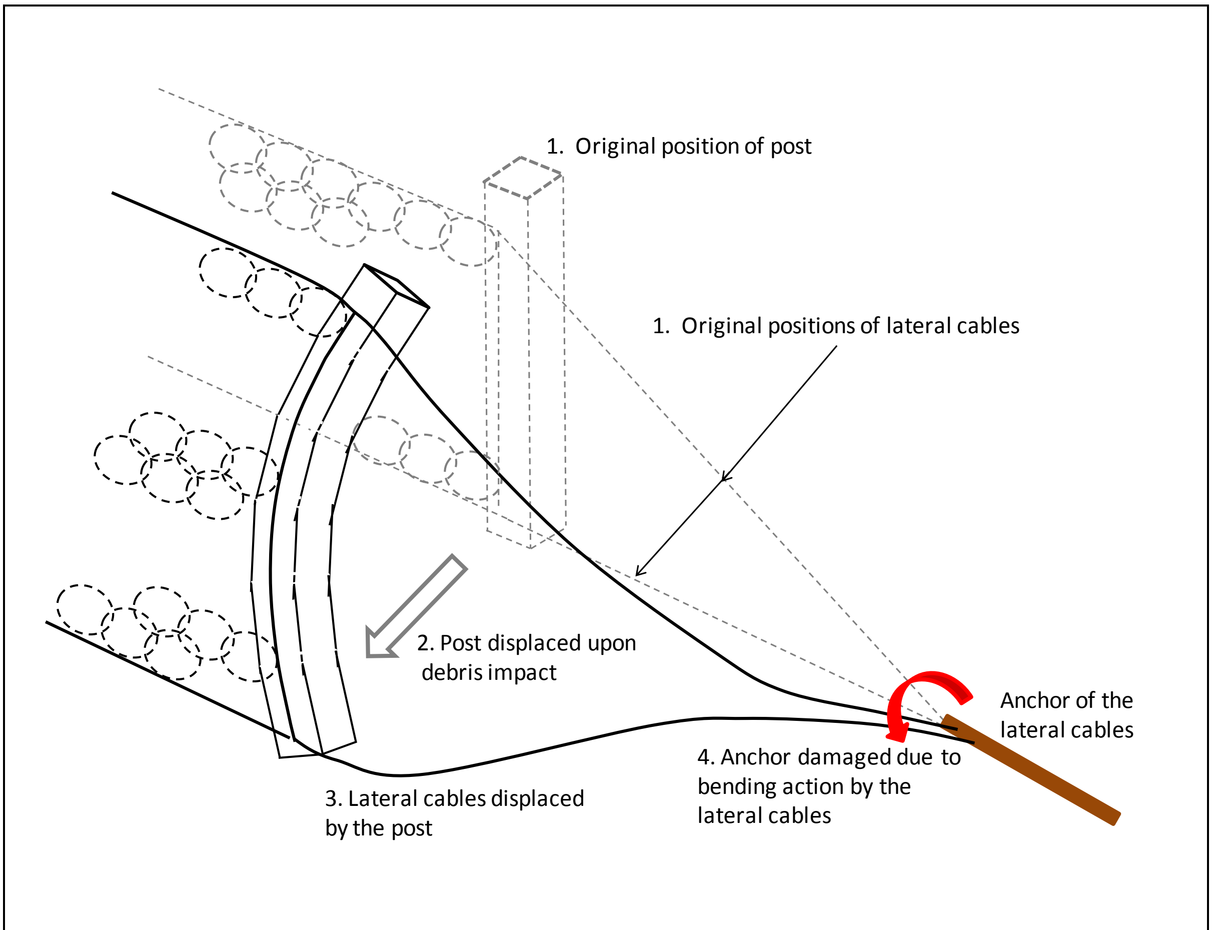

Figure 6.2 Bending of Lateral Anchor

Table of Contents Table of Contents Table of Contents Table of Contents

There have been reported case histories that flexible rockfall barriers intercepted snow avalanches in Europe. Although flexible rockfall barriers could stop certain type of snow avalanches, barriers were found damaged by snow avalanches of high energy level. Impact load patterns induced by snow avalanches and landslide debris could be similar. They could be both represented by areal loads. Some of the observations made by Margreth & Roth (2008), who examined some of the flexible rockfall barriers damaged by snow avalanches in Austria, are consistent with the present study. Margreth & Roth (2008) summarised their observations made over four winters from 2003 to 2006. They noted that barrier post foundations could be vulnerable to damage when barriers are subject to impact by snow avalanche, and recommended that post foundation should be properly reinforced and post spacing be reduced.

6.1 Further Work

It is acknowledge that the present preliminary back analyses only provided a relatively crude indication of the possible load transfer pattern of the flexible barrier through sensitivity analyses. It would be worthwhile to undertake more refined modelling work using advanced numerical tools to examine the structural response of the flexible barrier with due consideration of the post-failure mechanism, including possible load redistribution and progressive failure of the barrier system. Simulation of the interaction between the ground and the footings of the posts should also be considered in the future study. In the present case study, the foundations of two of the barrier posts failed upon the impact of landslide debris. The rigid connection at the post and the base plate could have played a role in this respect. Numerical analyses also indicate that the loading on the post foundations in the Jordan Valley barrier could have been up to about 350 kN to 450 kN which was liable to cause sliding failure. Attention to the loading on post foundation of barriers subjected to landslide debris impact is warranted in future research.

7 Conclusions

Preliminary back analyses of the structural response of a flexible barrier upon debris impact have been carried out using a non-linear structural program. The analyses appear to have reproduced some of the salient field observations. Sliding failure of the post foundation and buckling failure of the posts are inferred by the structural analysis. Given that there are no instrumented data (e.g. measured cable forces) for calibration purposes, the back calculated results cannot not be verified but they serve to provide a sensitivity analysis and give a feel of the possible behavior of flexible barrier upon debris impact. Through this study, some useful observations relevant to the design and detailing of flexible debris-resisting barriers are gained.

Instrumented field data or physical test results are pre-requisites for making advances in enhancing the fundamental understanding of the behaviour of flexible debris-resisting barriers. In addition, numerical tools that are capable of (i) assessing post-failure mechanism and energy dissipation of flexible barrier system, and (ii) accounting for the self-weight of debris retained in the bulged portions of ring nets would be useful for further review of this case history.

Table of Contents
Table of Contents
Table of Contents
Table of Contents

The preliminary back analyses provide a starting point to enhance the understanding of the possible structural response of flexible barriers subject to impact by landslide debris. It is intended to stimulate further thoughts and advances in respect of the subject.

8 References

Chan, S.L., Zhou, Z.H. & Liu, Y.P. (2012). Numerical analysis and design of flexible barriers allowing for sliding nodes and large deflection effects. *Proceedings of the One Day Seminar on Natural Terrain Hazard Mitigation Measures 2012*, AGS(HK), Hong Kong, pp 29-43.

GEO (2012). *Guidelines on Assessment of Debris Mobility for Open Hillslope Failures,* (Technical Guidance Note No. 34). Geotechnical Engineering Office, Hong Kong, 16 p.

Hungr, O. (2010). *Manual of DAN-W Release 10*. O. Hungr Geotechnical Research Inc., Canada, 61 p.

Kwan, J.S.H. & Sun, H.W. (2006). An improved landslide mobility model. *Canadian Geotechnical Journal*, vol. 43, pp 531-539.

LMM (2004). *Design for Installation of Rockfall Barriers for Development at Choi Wan Road and Jordan Valley Kowloon*, LMM Consulting Engineers Ltd., 304 p.

Margreth, S. & Roth, A. (2008). Interaction of flexible rockfall barriers with avalanches and snow pressure. Cold Regions Science and Technology, Vol. 51, pp 168-177.

Sun, W.H. & Law, R.P.H. (2012). *A Preliminary Study on Impact of Landslide Debris on Flexible Barriers* (GEO Technical Note No. TN 1/2012). Geotechnical Engineering Office, Hong Kong, 43 p.

Table of Contents
Table of Contents
Table of Contents
Table of Contents

Appendix A

Note of Landslide Inspection by
Landslide Investigation Consultants
(Reproduced from the Original Note)

Table of Contents
Table of Contents
Table of Contents
Table of Contents

Failure of Boulder Fence No. 11NE-A/ND8
above Slope No. 11NE-A/C872 near Choi Wan Road and Jordan Valley

1 General Information

1.1 The open hillslope failure (Incident No. LI/2009/12/2001) occurred on a west-facing hillside above Slope No. 11NE-A/C872 (Figure 1 and Plate 1). The failure volume was about 110 m^3. The landslide debris damaged an approximately 10 m section of boulder fence No. 11NE-A/ND8 (Plates 2 and 3).

1.2 The boulder fence is 5 m high and 128 m long. It was erected as part of the site formation project – Formation and Associated Infrastructure Works for Development at Choi Wan Road and Jordan Valley.

1.3 The boulder fence was designed by Scott Wilson Ltd in 2008. The design capacity is 1,000 kJ for retaining boulders up to 1 m^3. The equivalent impact velocity is 38.3 m/s for a 1 m diameter boulder. The supplier of the bounder fence is EI Montagne, and the fence was installed by Wai Luen Machine Works Company, the sub-contractor of the main contractor, China State Construction Engineering Corporation.

1.4 The failure was reported in December 2009. However, based on November 2007 and July 2008 aerial photographs, the failure was likely to have occurred during the heavy rainstorm in June 2008.

1.5 The failure is within the site boundary of the project which was still ongoing at the probable time of failure.

1.6 There is no past recorded landslide in the vicinity based on ENTLI and GEO's landslide database.

2 The Failure

2.1 The open hillslope failure occurred below an area of exposed rock outcrop with overhanging boulders. The scar measured approximately 18 m long by 10 m wide, up to 3.5 m deep (Figures 2 to 4). The displaced volume is about 110 m^3.

2.2 The upper portion of the source area comprises predominately saprolitic terrain, and is steeply inclined (> 50°) with adverse dipping joints (Figure 2 and Plate 4).

2.3 The lower portion of the source area comprises predominately matrix-supported debris overlying saprolite. The debris was dry at the time of inspection in December 2009. After the debris was removed, it can be seen that the lower portion of the landslide source area is sloping at 30° to 40°.

Table of Contents
Table of Contents
Table of Contents
Table of Contents

2.4 Deposition of the debris extends approximately 12 m from the toe of rupture on gently sloping (< 10°) ground. It consists of matrix-supported debris mixed with rounded to sub-rounded boulders and vegetation. Its thickness increases towards the frontal end from the rear end of deposition. No inspection was carried out during excavation of the debris. Therefore, it is unable to provide more details on the structure of the debris matrix. However, boreholes were sunk at the site for design of site formation works. The soil descriptions given in the borehole logs are silty, fine to coarse sand with some angular to subangular, fine to medium gravel sized quartz and granite fragments.

2.5 No signs of multiple surges of debris were observed. It is likely to have been a single surge impact by the landslide debris, which slid down the hillside as a whole lumped mass. Also, no sign of debris run-up against the fence was apparent.

3 The Boulder Fence

3.1 Boulder Fence No. 11NE-A/ND8 consists of two sections, both being 5 m high. The first section spans between posts Nos. P1 to P9 and P15 to the south, and the second section spans from post No. P10 to post No. P14 to the north. Debris from the probable June 2008 failure was within the first section, among the first three posts (i.e. posts Nos. P1, P2 and P15 at the southern end (Figure 1)). A sketch plan of this part of the boulder fence is shown in Figure 5 and the as-built drawings of the whole boulder fence system are given in Drawings Nos. P-010/AS/01 to 03.

3.2 The system comprises a netting, which is held up by a 20 mm diameter link cable supported on steel posts at 10 m apart. The netting is composed of circular steel rings of 350 mm in diameter and a wire mesh with an aperture of 25 mm × 25 mm. The link cable is secured in position by a shackle at both ends of the steel post (Figure 6), and fastened to the uphill anchor through an extension cable equipped with a braking system (Figure 8 and Plate 11). The braking system comprises four tailor-made steel plates each of which holds a 16 mm diameter steel extension rope in place and the steel plates are in turn secured in position with four 12 mm bolts. The extension ropes could move by up to 2.5 m if the load reaches a certain level.

3.3 Each steel post is made of square hollow sections (Figure 7) founded on a concrete pad foundation of 400 mm (L) x 400 mm (W) x 500 mm (D) (Drawing No. P-010/AS/03). The post is secured in position by 12 mm diameter guy ropes connecting to two downhill anchors and an upper anchor through half bent plates. The steel posts at both ends of the boulder fence are tied to the netting by stainless steel bands (Fig. X6.5, Drawing No. P-010/AS/02). Each end post is also supported by a lateral anchor equipped with the braking system.

3.4 The steel posts serve to keep the netting in upright position, and are not designed to take any direct impact from falling boulders or landslide debris. When boulder or debris hit the netting, the kinetic energy of the boulders or debris will be absorbed by the plastic deformation of the netting, and the frictional resistance from the extension of the rope in the brake elements at the uphill and lateral anchors.

Table of Contents Table of Contents Table of Contents Table of Contents

4 Failure of the Boulder Fence

4.1 The debris was contained by the first and second span of the boulder fence (Figure 1). The netting of the first and second span, together with the intermediate post (i.e. post No. P1), was pushed forward by the debris and displaced up to 2.2 m in the downslope direction (Figure 4). Post No. P1 was severely deformed (Plate 5). The other components of the system, which have been damaged as a result of the incident, included side post No. P15 in the south (Figure 3 and Plate 6) and the lateral anchor connected to post No. 15 (Plate 8). No apparent signs of damage or movement were observed on Post 2.

4.2 The deformed steel posts are shown in Plates 5 to 7. The foundations of Posts Nos. P1 and P15 also failed.

4.3 The head of the lateral anchor (connected to post No. P15) displaced about 1 m (Plate 8), leading to failure of the front part (about 0.9 m) of the grout (Plate 9). The half bent plate connected to the anchor head (Figure 8) remained intact. The extension ropes in the braking system were frayed and extended slightly (Plates 10 and 11). No significant lateral displacement of Post 1 was observed (Plate 5).

4.4 Post-failure inspection in April 2010 during the construction of the remedial works (which included the construction of a buttress (Plate 12) at the failure scar) found the remains of the braking system for the uphill anchor of post No. P15. No signs of damage were observed at the braking system.

5 Observations

5.1 Although the landslide debris severely damaged post No. P1 and pushed it some 2 m forward, the brake cable connecting post No. P1 and the uphill anchor did not appear to have extended significantly. This suggests that the impact energy of the debris has largely been absorbed by the deformation of the netting.

5.2 As the netting was deformed, the impact force due to the debris was transmitted to the end post No. P15 through the stainless steel bands (Fig. X6.5, Drawing No. P-010/AS/02), which fasten the netting to the end post. The stainless steel bands tend to behave as "rigid" connection restraining any movement of the net. This would have resulted in a large force being transmitted to post No. P15, causing failure of the steel post and its foundation, which are not designed to take any significant load. Consequently, post No. P15 deformed severely towards the direction of cable alignment and displaced about 1 m forward in the downhill direction. It is noted that in some other boulder fence systems (e.g. Geobrugg), the netting is not fixed to the end post.

5.3 There is no sign of direct impact of debris on the end post No. P15. Large forward displacement of the end post No. P15 due to the landslide debris would have resulted in a significant shear force on the lateral anchor (which acts almost perpendicular to the direction of the movement of the post), leading to bending of the anchor and local failure

Table of Contents
Table of Contents
Table of Contents
Table of Contents

of the surrounding grout. This may explain why despite there was a significant movement of the whole system of barrier, the brake elements were not mobilised.

5.4 The area in front of the barrier was inspected, and no noticeable evidence of landslide debris travelling beyond the secondary mesh of the flexible barrier (e.g. in the form of debris deposition or signs/marks left by landslide debris transportation in front of the barrier) has been observed.

by AECOM Asia Company Ltd.
under Landslide Investigation Consultancy Agreement No. CE41/2007(GE)
December 2010

Table of Contents
Table of Contents
Table of Contents
Table of Contents

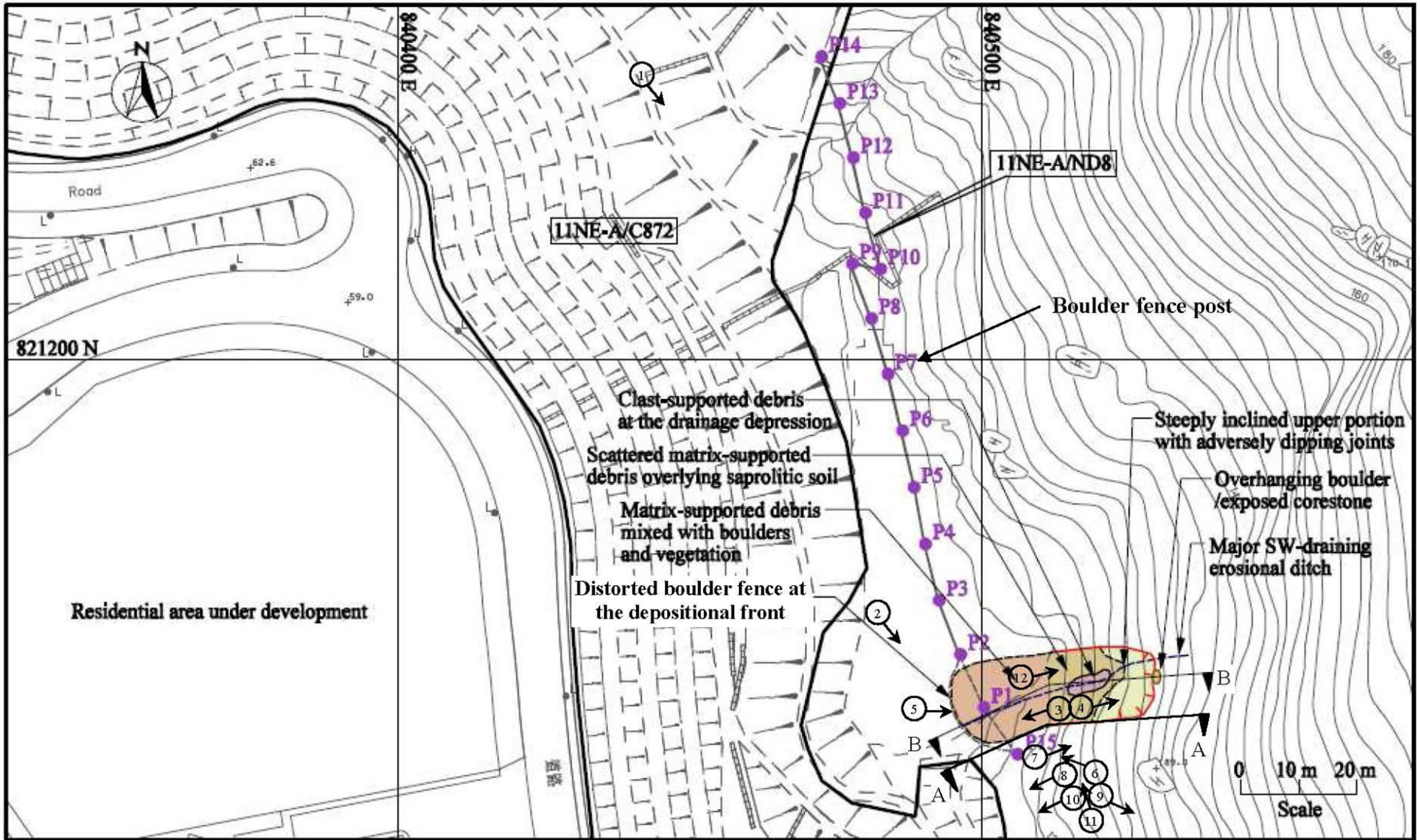

Note : Base plan is extracted from 1 : 1000 survey sheets Nos. 11NE-12B, 11NE-12D, 11NE-13A and 11NE-13C dated July 2009.

Figure 1 Location Plan

Table of Contents
Table of Contents
Table of Contents
Table of Contents

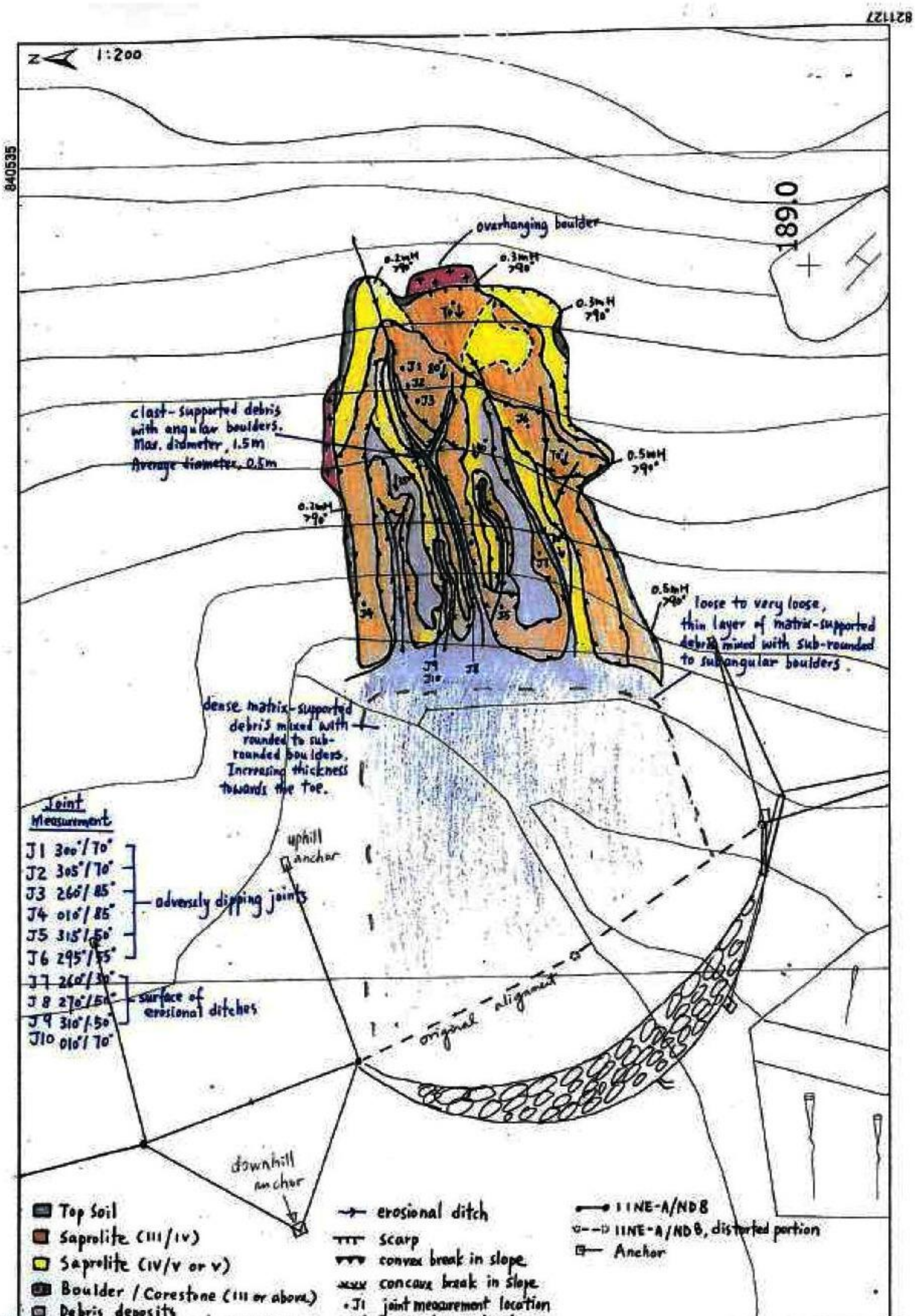

Figure 2 Sketch Plan of the Landslide

Table of Contents
Table of Contents
Table of Contents
Table of Contents

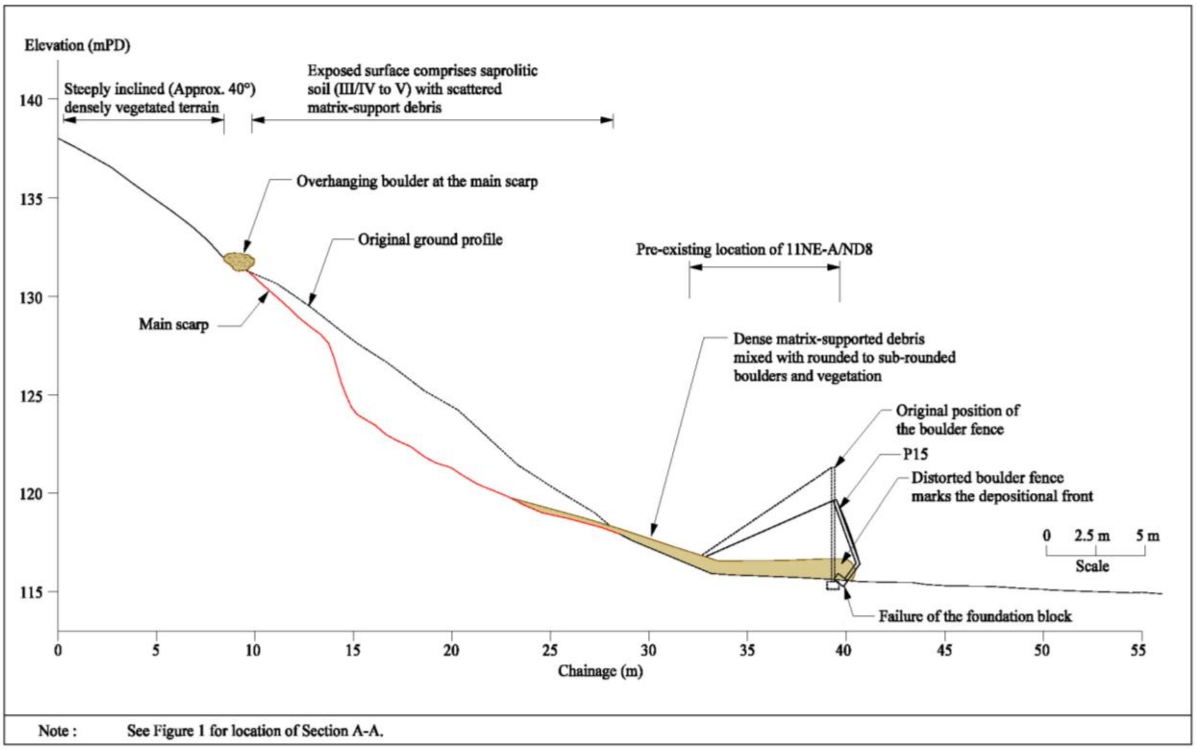

Figure 3 Section A-A through the Damaged End Post No. P15

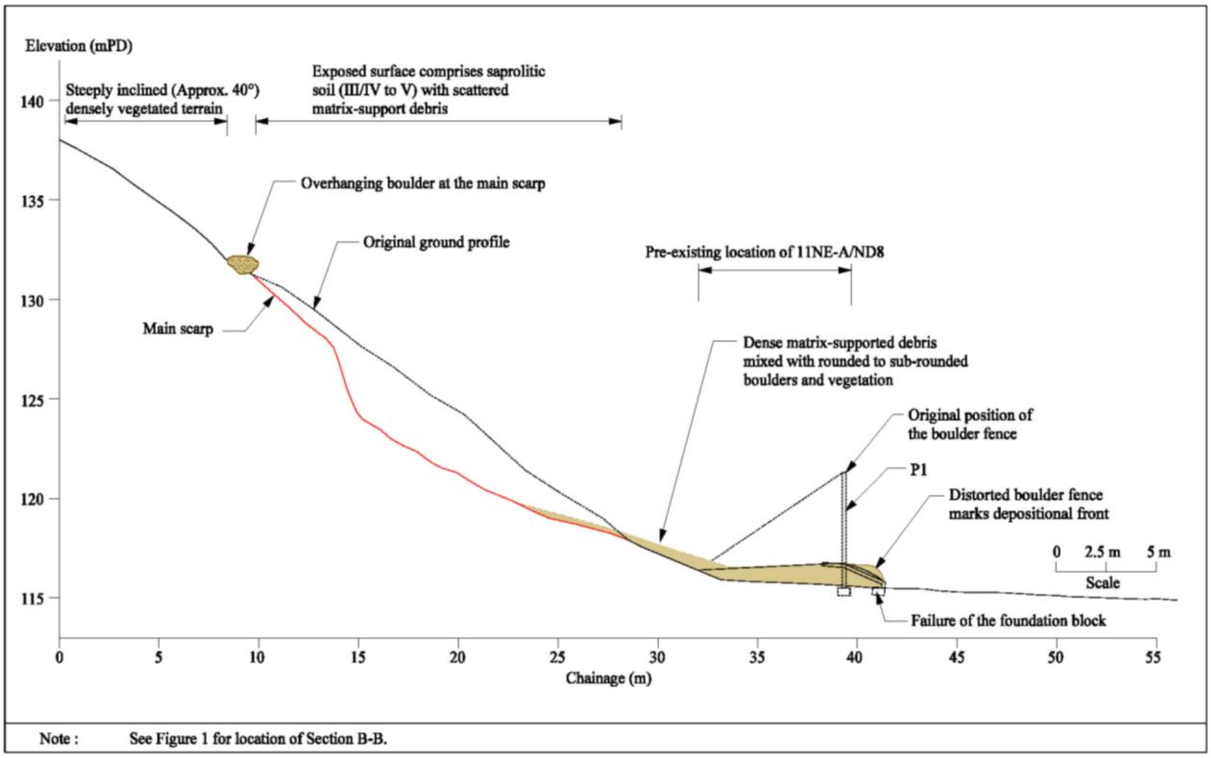

Figure 4 Section B-B through the Damaged Post No. P1

Table of Contents

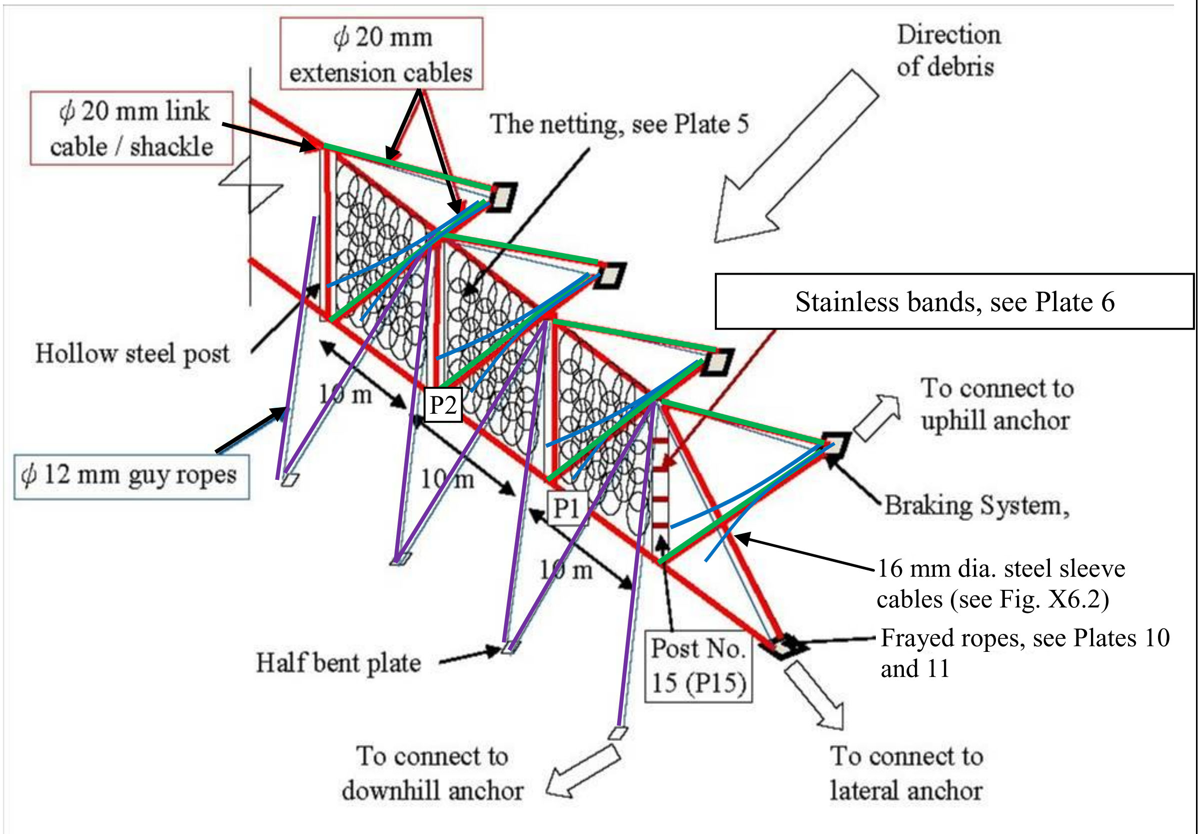

Figure 5 Sketch Plan of Boulder Fence at Posts Nos. P1 and P15

REP	ITEM
5	Shackle
8	Upper extension
11	Uphill wire guy rope
20	Downhill wire guy rope
21	Post
23	ASM net
28	Link cable / Shackle
29	Upper perimeter rope

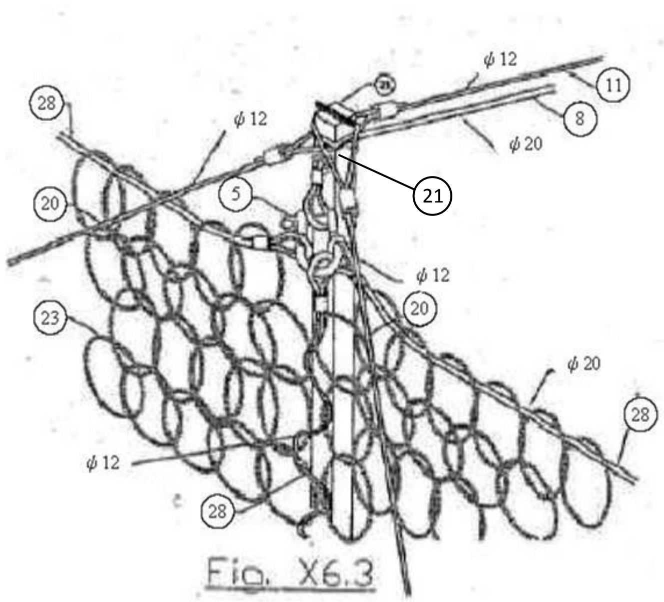

Figure 6 Details of the Arrangement at the Upper End of a Steel Post (Abstract of Fig. X6.3 from Drawing No. P-010/AS/02)

Table of Contents
Table of Contents
Table of Contents
Table of Contents

REP	ITEM
21	Galvanised post
22	Post stakes

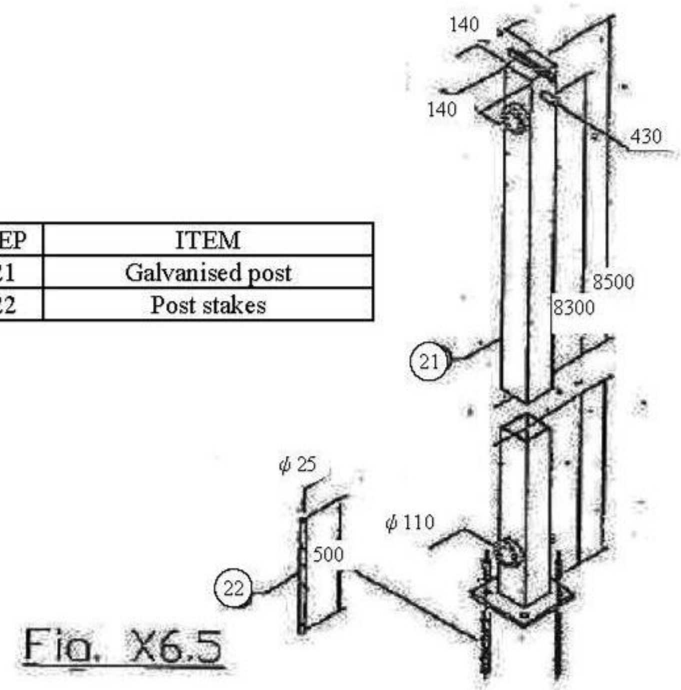

Figure 7 Details of Middle Steel Posts
(Abstract of Fig. X6.5 from Drawing No. P-010/AS/02)

REP	ITEM
1	Anchor bolt
5	Shackle
6	Monobloc brake
8	Upper extension cable
9	Lower extension cable
14	Wire rope clamp

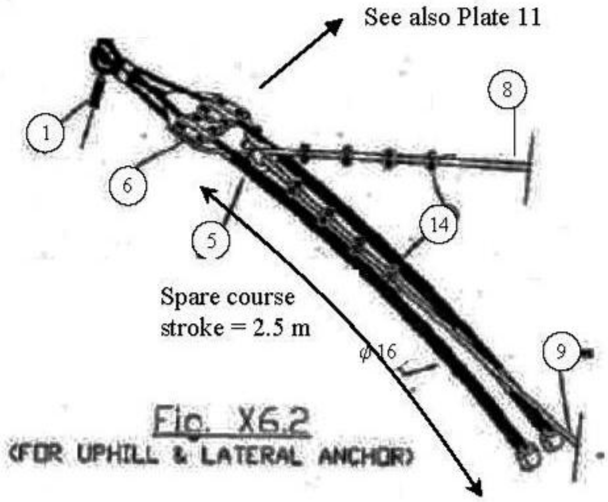

Figure 8 Details of Braking Systems for Uphill and Lateral Anchors
(Abstract of Fig. X6.2 from Drawing No. P-010/AS/02)

Table of Contents
Table of Contents
Table of Contents
Table of Contents

Plate 1 – Location of the Slope and Failed Boulder Fence

Plate 2 – General View of the Landslide

Plate 3 – View of Boulder Fence from the Landslide Source Area

Table of Contents
Table of Contents
Table of Contents
Table of Contents

Plate 4 – Upper Portion of the Landslide Source Area

Plate 5 – Steel Post No. P1 was Pushed Forward Together with the Netting

Table of Contents
Table of Contents
Table of Contents
Table of Contents

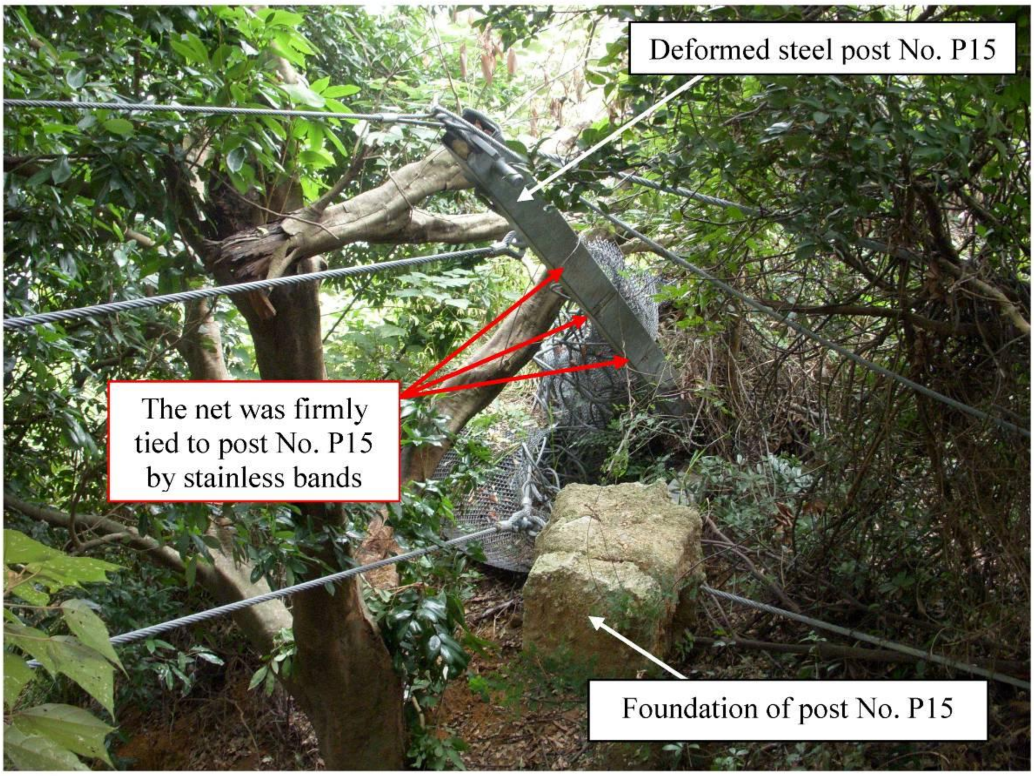

Plate 6 – Deformed End Post No. P15 and its Foundation

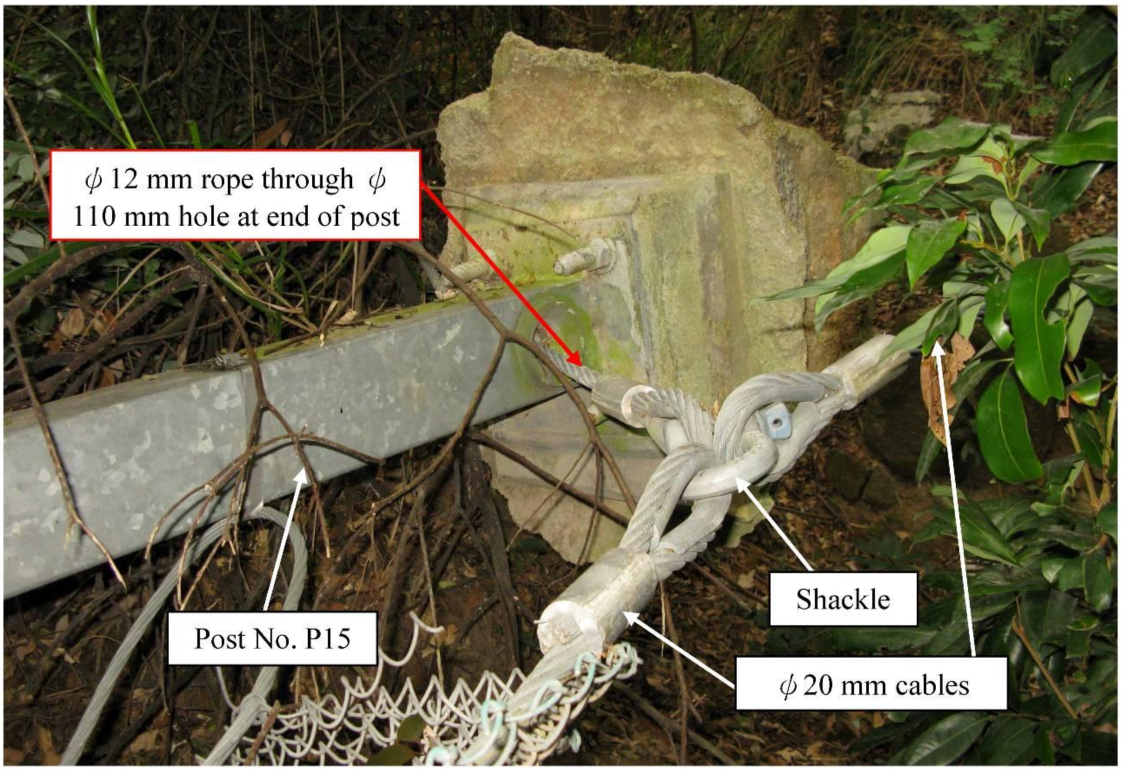

Plate 7 – Connection of Post No. P15 and its Foundation Block

Table of Contents
Table of Contents
Table of Contents
Table of Contents

Plate 8 – Location of Lateral Anchor

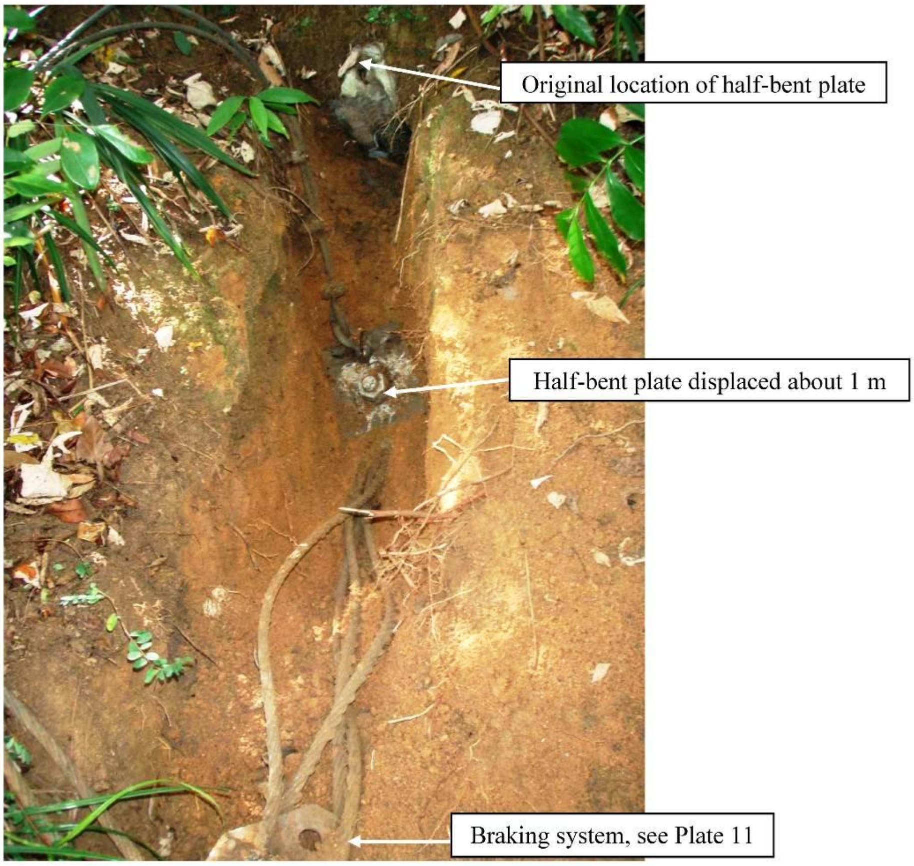

Plate 9 – Anchor Bent Leading to Failure of the Front Part of Grout Block

Table of Contents
Table of Contents
Table of Contents
Table of Contents

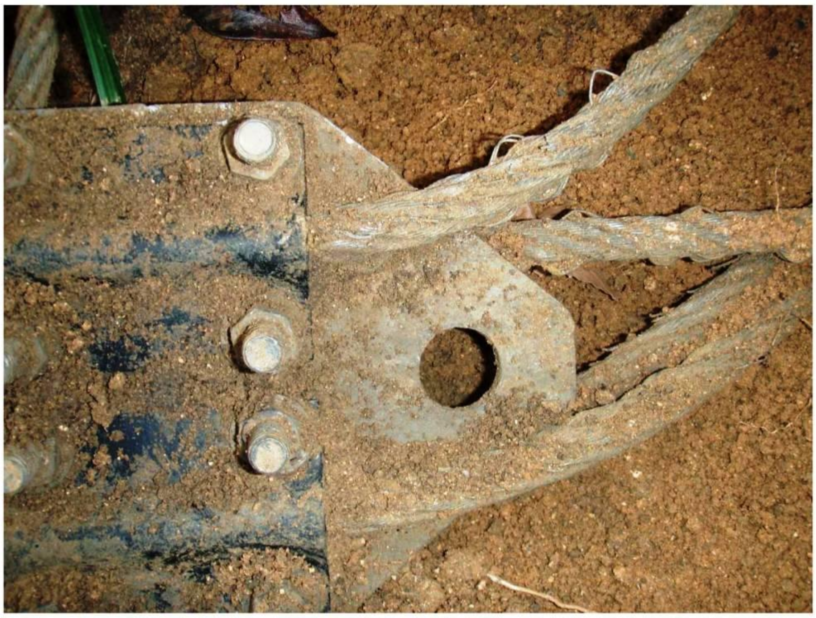

Plate 10 – Frayed Ropes Connected to the Braking System of the Lateral Anchor

Plate 11 – Ropes Might Have Been Extended Slightly at the Monobloc Brake Connected to the Lateral Anchor

Table of Contents
Table of Contents
Table of Contents
Table of Contents

Plate 12 – Remedial Works for the Landslide Scar

Table of Contents
Table of Contents
Table of Contents
Table of Contents

Post Coordinates

Post No.	E-Coordinate	N-Coordinate
P1	840500.369	821140.387
P2	840496.355	821149.461
P3	840492.714	821158.734
P4	840490.325	821168.367
P5	840488.394	821178.083
P6	840486.430	821187.766
P7	840483.934	821197.488
P8	840481.130	821207.023
P9	840477.817	821216.378
P10	840482.675	821215.488
P11	840480.076	821225.098
P12	840477.995	821234.563
P13	840475.663	821243.862
P14	840472.573	821251.870
P15	840506.145	821132.370

Drg. No. P-010/AS/01

Table of Contents
Table of Contents
Table of Contents
Table of Contents

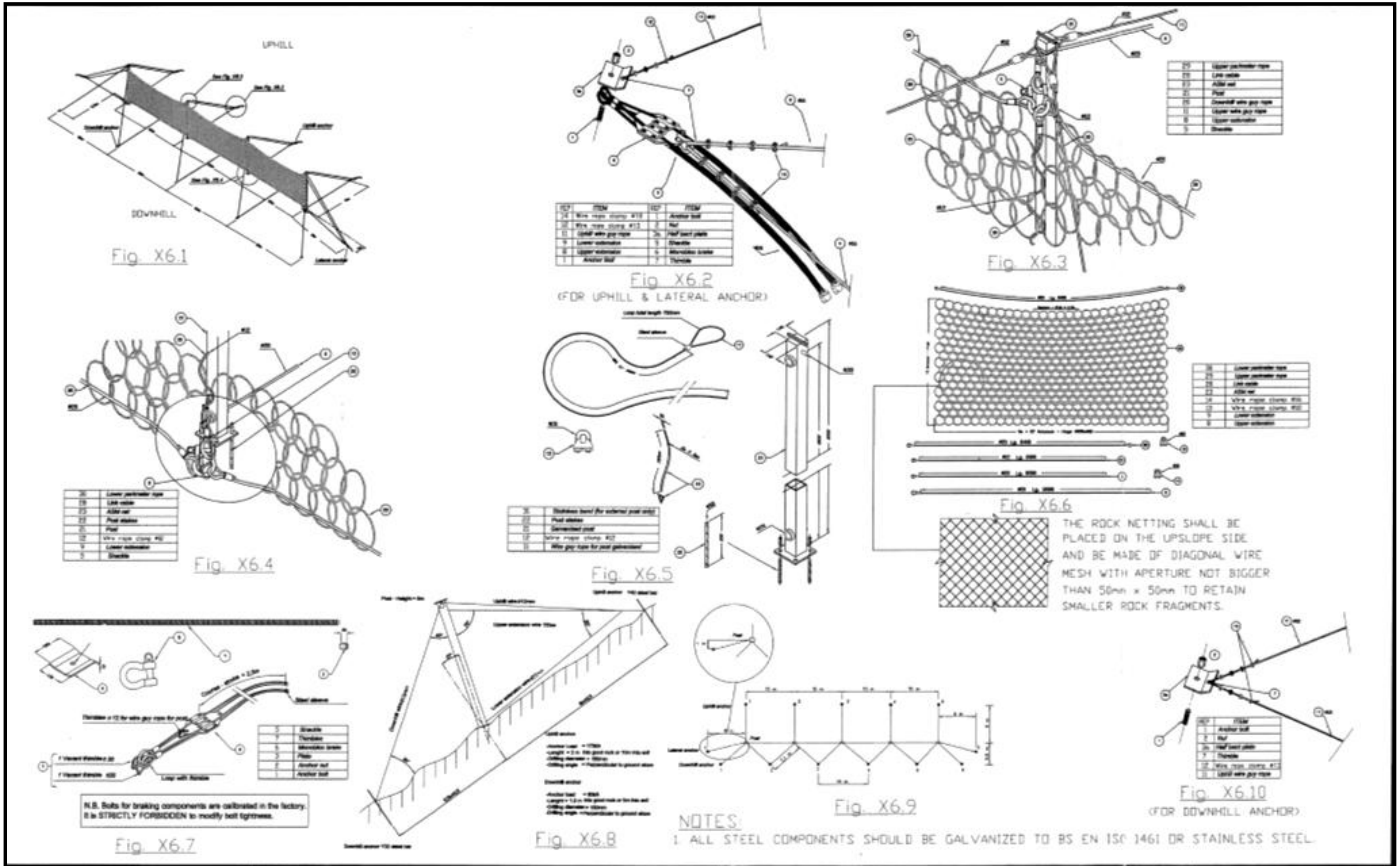

LMM Consulting Engineers	Project: Development at Choi Wan Road and Jordan Valley Kowloon	Title: Rockfall Barriers Design Details (I)	SCALE: as shown DATE: Mar., 2004 FIG: 6

Drg. No. P-010/AS/02

NOTE FOR ANCHOR BARS:

1. ANCHOR BARS GENERAL

1.1 AN ANCHOR BAR SHALL CONSIST OF A STEEL BAR, CEMENT GROUT, CENTRALIERS, COUPLERS, HEAD ASSEMBLY AND ALL OTHER ASSOCIATED COMPONENTS AS SPECIFIED IN THE RELEVANT DRAWINGS. WHERE INDICATED ON THE DRAWINGS ANCHOR BARS AND STEEL COMPONENTS SHALL BE HOT DIP GALVANISED TO BE BS729: 1971 AS A PROTECTIVE TREATMENT.

1.2 STEEL BARS SHALL COMPLY WITH BS4449 & CS2, 1995.

1.3 THE CONTRACTOR SHALL SUBMIT, 2 WEEKS PRIOR TO COMMENCING DRILLING FOR ANCHOR BARS, TO THE ENGINEER THE PROPOSED METHOD OF ANCHOR BAR INSTALLATION, DETAILS OF THE TESTING ASSEMBLY, INCLUDING, INTER ALIA, JACKS, SUPPORTS, MEASURING APPARATUS AND ANY OTHER DETAILS NECESSARY FOR PERFORMING THE TEST. DRILLING RECORDS OF ANCHOR BAR HOLES SHALL BE PROVIDED TO THE ENGINEER BEFORE INSTALLATION.

1.4 Y40-'Y' DENOTES HIGH YIELD BAR WITH ULTIMATE YIELD STRENGTH = 460MPA.

2. INSTALLATION

2.1 ALL VEGETATION AND DEBRIS ON EXISTING WALL SURFACE SHALL BE CLEARED.

2.2 AIR SHALL BE USED AS DRILLING MEDIUM, DRILLHOLES SHALL BE CLEARED OF ALL DEBRIS IMMEDIATELY BEFORE GROUTING. BEFORE THE ANCHOR BARS ARE INSTALLED, THE CONTRACTOR SHALL FURNISH THE ENGINEER WITH ALL NECESSARY EQUIPMENT AND ASSISSTANCE TO CHECK THE INCLINATION, BEARING, CLEANLINESS AND LENGTH OF ALL DRILLHOLES.

2.3 IF COLLAPSE OF SOIL IN DRILLHOLE IS FOUND OR GROUNDWATER IS ENCOUNTERED DURING THE DRILLING PROCESS, DRILLING OF THE SUBSEQUENT ANCHOR BARS SHALL BE MADE WITH CASING IN ADVANCE OF DRILLING. THE CASING SHOULD ONLY BE REMOVED IMMEDIATELY BEFORE OR SIMULTANEOUSLY WITH THE GROUT OPERATION.

3. DIMENSIONAL TOLERANCE

3.1 THE INSTALLATION OF ANCHOR BARS SHALL COMPLY WITH THE FOLLOWING DIMENSIONAL TOLERANCES.-

(A) THE HORIZONTAL AND VERTICAL PORTIONS OF THE NAIL HEADS AND THE ORIENTATION OF STEEL BARS SHALL NOT EXCEED 5% OF THE HOLE LENGTH.

(B) AT ALL PLACES A MINIMUM OF 10mm GROUT COVER TO THE SOIL BARS AND COUPLERS SHALL BE ACHIEVED.

4. GROUT FOR ANCHOR BARS

4.1 CEMENT GROUT USED TO FIX ANCHOR BARS SHALL COMPLY WITH THE FOLLOWING REQUIREMENTS:-

(A) UNLESS OTHERWISE APPROVED, CEMENTS USED FOR GROUTING SHALL COMPLY WITH BS12.

(B) THE GROUT MIX PROPORTIONS AND THE TYPE OF ADDITIVE, IF ANY, SHALL BE SUBMITTED FOR APPROVAL BY THE ENGINEER AT LEAST THREE DAYS PRIOR TO COMMENCEMENT OR GROUTING. THE GROUT SHALL HAVE A WATER CEMENT RATIO NOT EXCEEDING 0.45.

(C) THE GROUT MIX SHALL NOT BE SUBJECTED TO BLEEDING IN EXCESS OF 0.5% BY VOLUME 3 HOURS AFTER MIXING OR 1% MAXIMUM WHEN MEASURED AT 20° C IN A COVERED GLASS OR METAL CYLINDER OF 100mm INTERNAL DIAMETER AND WITH A GROUT DEPTH OF APPROXIMATELY 100mm. IN ADDITION, THE WATER SHALL BE REABSORBED WITHIN 24 HOURS.

(D) BATCHING OF THE DRY MATERIALS SHALL BE BY WEIGHT. THE AMOUNT OF WATER USED SHALL BE MEASURED BY A CALIBRATED FLOWMETER OR A MEASURING TANK.

(E) THE PROCEDURE TO FOLLOWED FOR MIXING THE GROUT SHALL BE THAT APPROXIMATELY TWO THIRDS OF THE CEMENT SHALL BE ADDED TO THE WATER FOLLOWED BY THE ADDITIVE, IF ANY, FOLLOWED BY THE REMAINING THIRD OF CEMENT. ANY ALTERNATIVE MIXING PROCEDURES PROPOSED BY THE CONTRACTOR SHALL BE AGREED BY THE ENGINEER. THE GROUT SHALL BE MIXED IN A HIGH SPEED COLLOIDAL GROUT MIXER WITH A MINIMUM SPEED OF 1000 RPM. THE GROUT SHALL BE MIXED FOR A SUFFICIENT TIME TO PRODUCE A GROUT OF UNIFORM CONSISTENCY.

(F) AFTER MIXING, THE GROUT SHALL BE KEPT CONTINUOUSLY AGITATED. THE GROUT SHALL BE PASSED THROUGH A NOMINAL 1.2mm SIEVE PRIOR TO INJECTION. THE GROUT SHALL BE USED AS SOON AS POSSIBLE AFTER MIXING AND IN ANY CASE WITHIN 30 MINUTES OF ADDING CEMENT UNLESS SPECIAL RETARDING AGENTS ARE USED.

(G) THE PUMP USED FOR GROUT INJECTION SHALL BE OF THE POSITIVE DISPLACEMENT TYPE.

(H) AFTER MIXING AND SIEVING THE PRIOR TO INJECTION THE GROUT SHALL BE SAMPLED AND TESTED IN ACCORDANCE WITH US CORPS OF ENGINEERS (FLOW-CONE METHOD) CRD-C 79-58. EXCEPT WITH THE PRIOR AGREEMENT OF THE ENGINEER FOR GROUTS CONTAINING ADDITIVES, GROUT HAVING AN EFFLUX TIME OF LESS THAN 15 SECONDS SHALL BE REJECTED.

(I) GROUT CUBES SHALL BE PREPARED, CURED AND TESTED IN ACCORDANCE WITH BS1881 USING 100mm CUBES. NINE CUBES SHALL BE MADE EACH TIME WHEN THERE IS A GROUTING OPERATION. GROUT CUBE STRENGTHS, THREE EACH FOR THREE SEVEN AND TWENTY EIGHT DAYS SHALL BE OBTAINED FOR EACH SET OF NINE SAMPLES TAKEN. GROUT CUBE STRENGTH SHALL BE AT LEAST 30MPA AT TWENTY EIGHT DAYS.

(J) ADDITIVES AND ADMIXTURES SHALL COMPLY WITH THE REQUIREMENTS OF BS5075 (1974) AND SHALL ONLY BE USED WITH THE PRIOR AGREEMENT OF THE ENGINEER.

5. PULL-OUT TESTS

5.1 WHEN REQUIRED BY THE ENGINEERS OR AS SPECIFIED IN THE DRAWINGS, PULL-OUT TESTS SHALL BE CARRIED OUT ON TRIAL ANCHOR BARS WHICH SHALL BE INSTALLED AND TESTED PRIOR TO THE INSTALLATION OF PERMANENT ANCHOR BARS AS DIRECTED BY THE ENGINEER. ANCHOR BARS SUBJECTED TO PULL-OUT TESTS SHALL NOT CONFORM PART OF THE PERMANENT WORKS. DRILLING RECORDS OF HOLES SELECTED FOR PULL-OUT TESTS SHALL BE PROVIDED TO THE ENGINEER. THE FOLLOWING PROCEDURES FOR PULL-OUT TESTS SHALL BE ADOPTED:-

(A) THE ANCHOR BARS SHALL BE GROUTED OVER THE LENGTH AS SPECIFIED IN THE DRAWINGS OR AS DIRECTED BY THE ENGINEER. THE PULL-OUT TESTS SHALL NOT BE CARRIED OUT UNTIL THE GROUT HAS REACHED ITS CUBE STRENGTH OF 30MPA.

(B) THE TEST LOAD (TP) SHALL BE 1.6 TIMES THE WORKING LOAD AS SPECIFIED IN THE DRAWINGS.

(C) AN INITIAL LOAD (TA) EQUALS TO 5% OF (TP) SHALL BE APPLIED. THE RANGE BETWEEN TA AND TP SHALL BE DIVIDED INTO THREE EQUAL STEPS OF MAGNITUDE T.

(D) A PROGRAMME OF THREE LOADING AND UNLOADING CYCLES SHALL THEN BE CARRIED OUT WITH THE LOAD BEING INCREASED FROM TA IN SUCCESSIVE CYCLES BY T, 2T UP TO TP. AFTER THE PEAK LOADING IN EACH CYCLE IS REACHED, MEASUREMENTS OF THE DEFORMATION INCREASE WITH THE LOAD HELD CONSTANT SHALL BE TAKEN FOR 60 MINUTES. WHEN REQUIRED THE LOAD SHALL BE HELD LONGER AS DIRECTED BY THE ENGINEER.

(E) AFTER THE ABOVE MEASUREMENTS HAVE BEEN TAKEN FOR EACH CYCLE, THE LOAD SHALL THEN REDUCED TO TA AND THE EXTENSION RECORDED. AFTER THAT, WHERE REQUIRED BY THE ENGINEER, THE WHOLE ANCHOR BAR SHALL THEN BE PULLED OUT FROM THE DRILLED HOLE FOR THE ENGINEER'S INSPECTION. UNLESS OTHERWISE INSTRUCTED BY THE ENGINEER, THE DRILLED HOLE SHALL BE FILLED BY GROUTING.

(F) IF THE ANCHOR BAR CANNOT BE PULLED OUT WITHOUT EXCEEDING THE MAXIMUM ALLOWABLE TEST LOAD AS SPECIFIED IN (G), THEN THE BAR SHALL BE CUT-OFF FLUSH WITH THE FINISHED GROUND AND REMAINING PART OF THE DRILLHOLE GROUTED.

(G) THE MAXIMUM ALLOWABLE TEST LOAD SHALL NOT EXCEED 80% OF THE ULTIMATE TENSILE STRENGTH OF THE STEEL BAR FORMING THE ANCHOR BAR. UNLESS OTHERWISE INSTRUCTED BY THE ENGINEER, ANY PROTRUSIONS FROM THE DRILLHOLE SHALL BE CUT OFF AND THE DRILLHOLE SHALL THEN FILLED BY GROUTING.

(H) THROUGHOUT THE TEST, THE ANCHOR BAR MOVEMENT VERSES THE APPLIED LOAD SHALL BE MEASURED AND PLOTTED ON A GRAPH. ALL THE RESULTS SHALL BE SUBMITTED TO THE ENGINEER WITHIN 3 DAYS OF COMPLETION OF THE TEST.

(I) TRIAL ANCHOR BAR SHALL BE PROVIDED FOR PULL-OUT TEST AT LOCATIONS AS DIRECTED BY THE ENGINEER AS SCHEDULED BELOW.-

PULL-OUT TEST SCHEDULE FOR ANCHOR BAR

TRIAL ANCHOR BAR MARK	MAX. TEST LOAD (KN)	DESIGN LOAD (kN)	EMBEDDMENT LENGTH OF ANCHOR BARS (M)	GROUT LENGTH OF THE ANCHOR BARS (M)	LOCATION
2 NOS. FOR UPHILL ANCHOR	272	170	MINIMUM. 10M IN CDG OR 2M IN ROCK	MINIMUM. 10M IN CDG OR 2M IN ROCK	UPHILL ANCHOR (UA1-UA14)
2 NOS. FOR LATERAL ANCHOR	272	170	MINIMUM. 10M IN CDG OR 2M IN ROCK	MINIMUM. 10M IN CDG OR 2M IN ROCK	LATERAL ANCHOR (LA1-LA4)
2 NOS. FOR DOWNHILL ANCHOR	128	80	MINIMUM. 8M IN CDG OR 1.5M IN ROCK	MINIMUM. 8M IN CDG OR 1.5M IN ROCK	DOWNHILL ANCHOR (DA1-DA12)

REMARK: THE TRIAL TEST LOCATION SHALL BE DETERMINED ON SITE BY THE ENGINEER PRIOR TO CARRYING OUT TESTING.

THE ACCEPTANCE CRITERIA FOR PULL-OUT TEST :
THE EXTENSION OF THE STEEL BARS SHOULD NOT EXCEED 0.2% OF THE GROUT LENGTH.

6. MEASUREMENT ACCURACY

6.1 THE APPARATUS FOR MEASURING LOADS AND DEFORMATIONS SHALL HAVE AN ACCURACY OF 2 KN AND 0.05mm RESPECTIVELY.

7. SCHEDULE OF ANCHOR BARS (ø150mm DRILLHOLE WITH Y40/Y32 STEEL BAR) REFER TO TABLE 1

TABLE 1 : FOUNDATION SCHEDULE OF ROCKFALL BARRIER

ANCHOR LOCATION	ANCHOR NO.	DESIGNED ANCHOR LOAD	ANCHOR TYPE	MINI. EMBEDDMENT LENGTH OF ANCHOR BAR, m	INCLINED ANGLE WITH HORIZONTAL	DRILLHOLE DIAMETER	Reference Borehole
Uphill Anchor with Friction Brake	UA1-UA14	170 KN	Y40mm Galvanized Steel Bar	Minimum 10m into soil or 2m into rock (Grade III or better rock)	15°	150mm	BH1-BH4
Side Anchor with Friction Brake	LA1-LA4	170 KN	Y40mm Galvanized Steel Bar	Minimum 10m into soil or 2m into rock (Grade III or better rock)	35°	150mm	BH1-BH4
Downhill Anchor without Friction Brake	DA1-DA12	80 KN	Y32mm Galvanized Steel Bar	Minimum 5m into soil or 1.5m into rock (Grade III or better rock)	65°	150mm	BH1-BH4

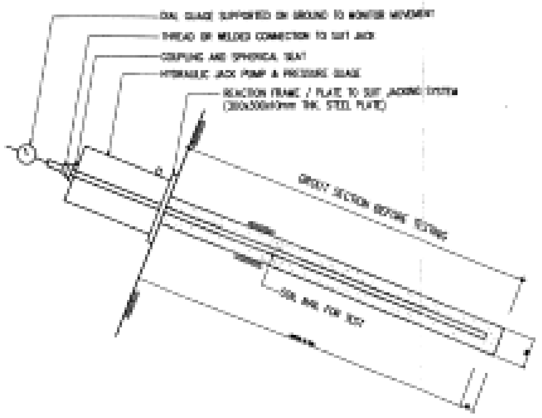

TYPICAL DETAILS FOR ANCHOR PULL-OUT TEST

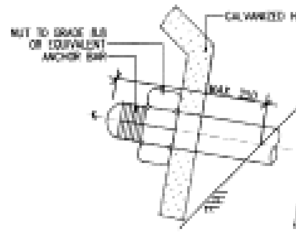

DETAIL "B"

NOTES : 1. GALVANIZED STEEL TO BS729
2. STEEL PLATE TO BS4360

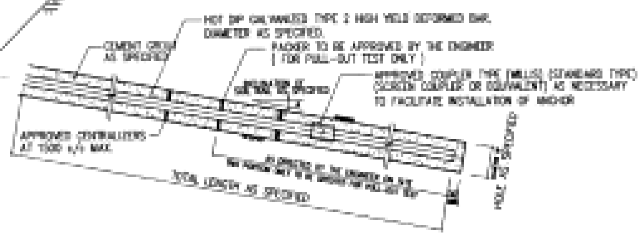

GENERAL ARRANGEMENT OF STEEL BAR ANCHOR

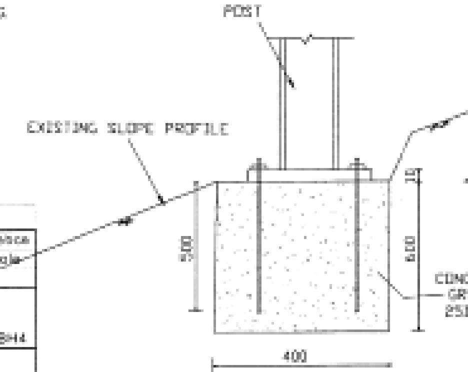

SECTION 1-1

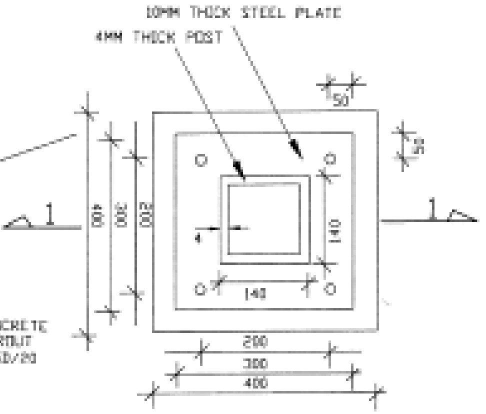

DETAIL "B"

POST BASE FOUNDATION

LMM Consulting Engineers	Project: Development at Choi Wan Road and Jordan Valley Kowloon	Title: Rockfall Barriers Design Details & Notes For Anchor Bars	SCALE : - DATE : Mar., 2004 FIG. : 7

Table of Contents
Table of Contents
Table of Contents
Table of Contents

Appendix B

Structural Analysis

Table of Contents
Table of Contents
Table of Contents
Table of Contents

Contents

Table of Contents
Table of Contents
Table of Contents

List of Tables

Table of Contents
Table of Contents
Table of Contents

List of Figures

Table of Contents
Table of Contents
Table of Contents

B.1 Introduction

A flexible barrier system exhibits a highly non-linear structural behavior. A non-linear finite element program “NIDA-MNN Version 8.0” developed by the Hong Kong Polytechnic University was used in this study. Details of the program and validation of the program against field testing of instrumented flexible barriers are reported by Chan et al (2012). According to the program developer, NIDA-MNN is capable of analysing large deformations of structural elements, such as ring net and cables, and large elasto-plastic deformations of brake elements by considering structural deformations in the iterations of the force equilibrium calculations (Chan et al, 2012).

B.2 Method of Back Analysis

In the structural analysis, sliding cable elements have been used for simulation of ring nets and rope cables. The analysis model is three-dimensional comprising two panels of the flexible barrier impacted by landslide debris. Both geometrical non-linearity and material non-linearity are considered.

B.3 Structural Components

The flexible rockfall barrier system consists of ring nets, hollow steel posts, energy dissipating devices, rope cables and ground anchor at end supports as shown in Figure 5 of Appendix A. Details of structural components are given below:

Ring net

(1) Diameter of ring: 350 mm
(2) Diameter of ring wire: 3 mm (7 spirals)
(3) Six rings connection

Hollow steel post

(1) Height: 5 m
(2) Size: 140 mm x 140 mm
(3) Thickness: 4 mm
(4) Radius of gyration: 55.2 mm
(5) Cross section area = 2.14×10^3 mm^2
(6) Second moment of area = 6.52×10^6 mm^4
(7) Section modulus = 93.1×10^3 mm^3
(8) Yield stress = 235 MPa
(9) Elastic modulus = 200 GPa
(10) Founded on shallow concrete footing
of dimensions 400 mm x 400 mm x 500 mm depth

Energy dissipating device (brake element)

Refer to Figure B1 for the force and displacement characteristic curve.

Table of Contents
Table of Contents
Table of Contents
Table of Contents

Extension rope cables

(1) Diameter of top rope cable is 20 mm (6 threads of 19 wires)
(2) Diameter of bottom rope cable is 20 mm (6 threads of 19 wires)
(3) Tensile failure load is 270 kN.

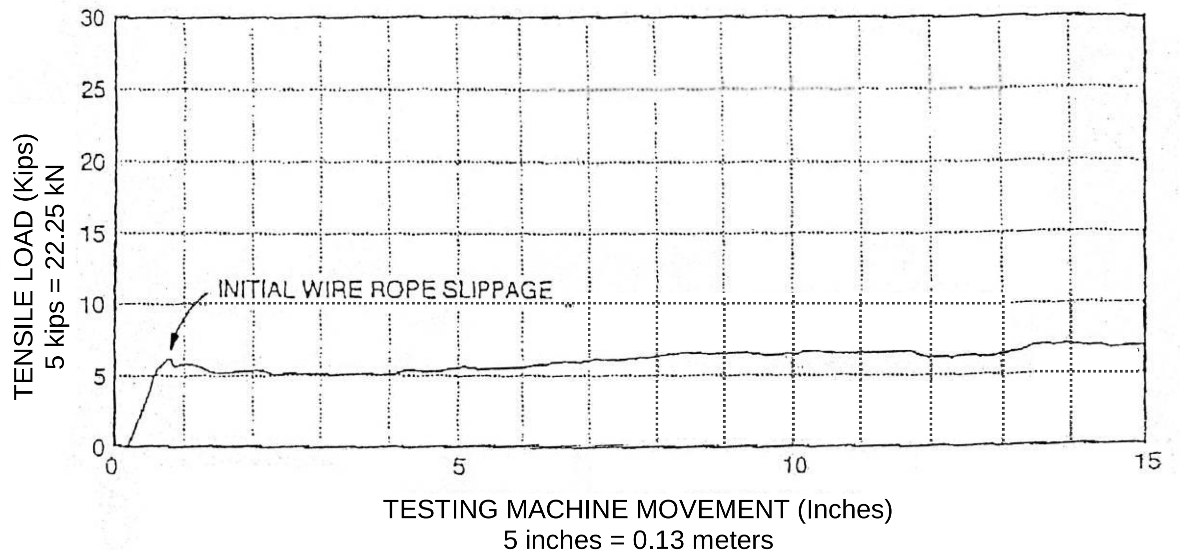

Figure B1 Force - Displacement Characteristic Curve of Energy Dissipating Device

B.4 Structural Modelling

In the analysis, the connection point between every two ring nets is moveable. This is achieved by using sliding cable elements. Similarly, the sliding cable elements are also used to model the extension of the rope cables. A sliding cable element is a group of conventional cable elements that dynamically pass through a number of prescribed nodes which can be either fixed or movable (see Figure B2), and it takes tension only. The tension force along the length of the cable at any segment is the same, since frictional force acting on the cable is not considered in the analysis.

Table of Contents
Table of Contents
Table of Contents
Table of Contents

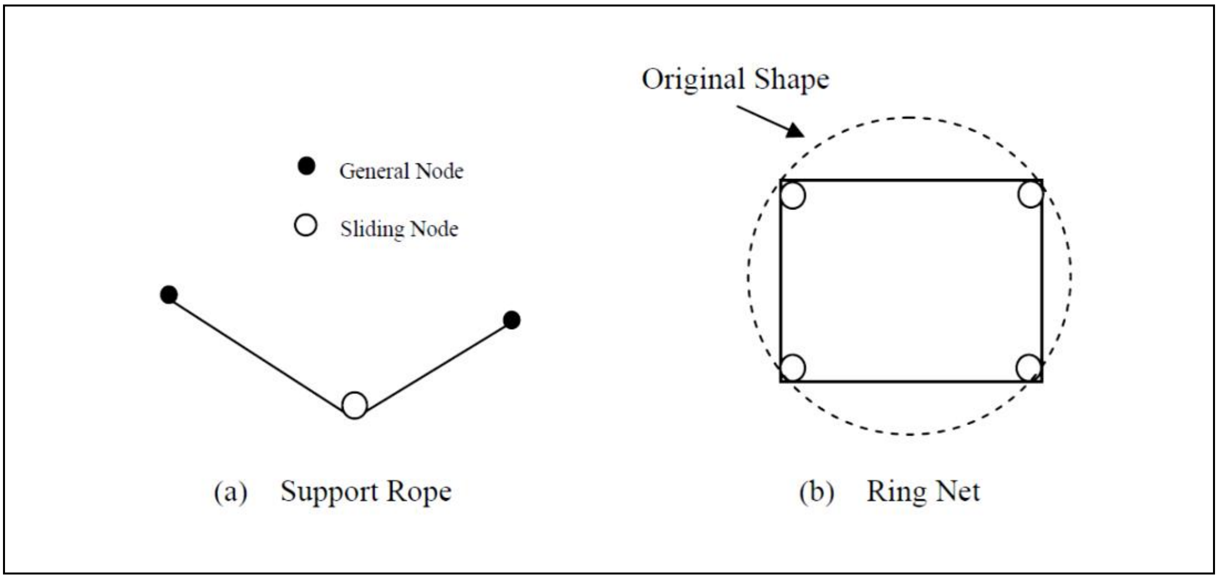

Figure B2 Sliding Cable Element for Support Rope and Ring Net (Zhou & Chan, 2011)

The energy dissipating devices exhibit non-linearity in terms of both geometrical and material behaviour. The energy dissipating devices attached to the uphill cables were not activated as observed in the site inspections. This could have been related to the friction developed at the connection between the uphill cables and the posts. The brake elements attached to the uphill rope cables were therefore not included in this analysis.

The post foundation is modelled as a pin support, since the shallow footing could not have provided a high rotational restraint. This agrees with the site observation that the footings of Posts P1 and P15 significantly rotated following the impact of the landslide debris. Due to the limitation of the computer program, simulations of the post failure, e.g. sliding of the footing, is not allowed.

The two panels of the rockfall barrier spanning across Posts P1, P2 and P15, which were struck by landslide debris, are considered in the numerical analysis. The model set-up and assumed boundary conditions are shown in Figure B3.

Table of Contents
Table of Contents
Table of Contents
Table of Contents

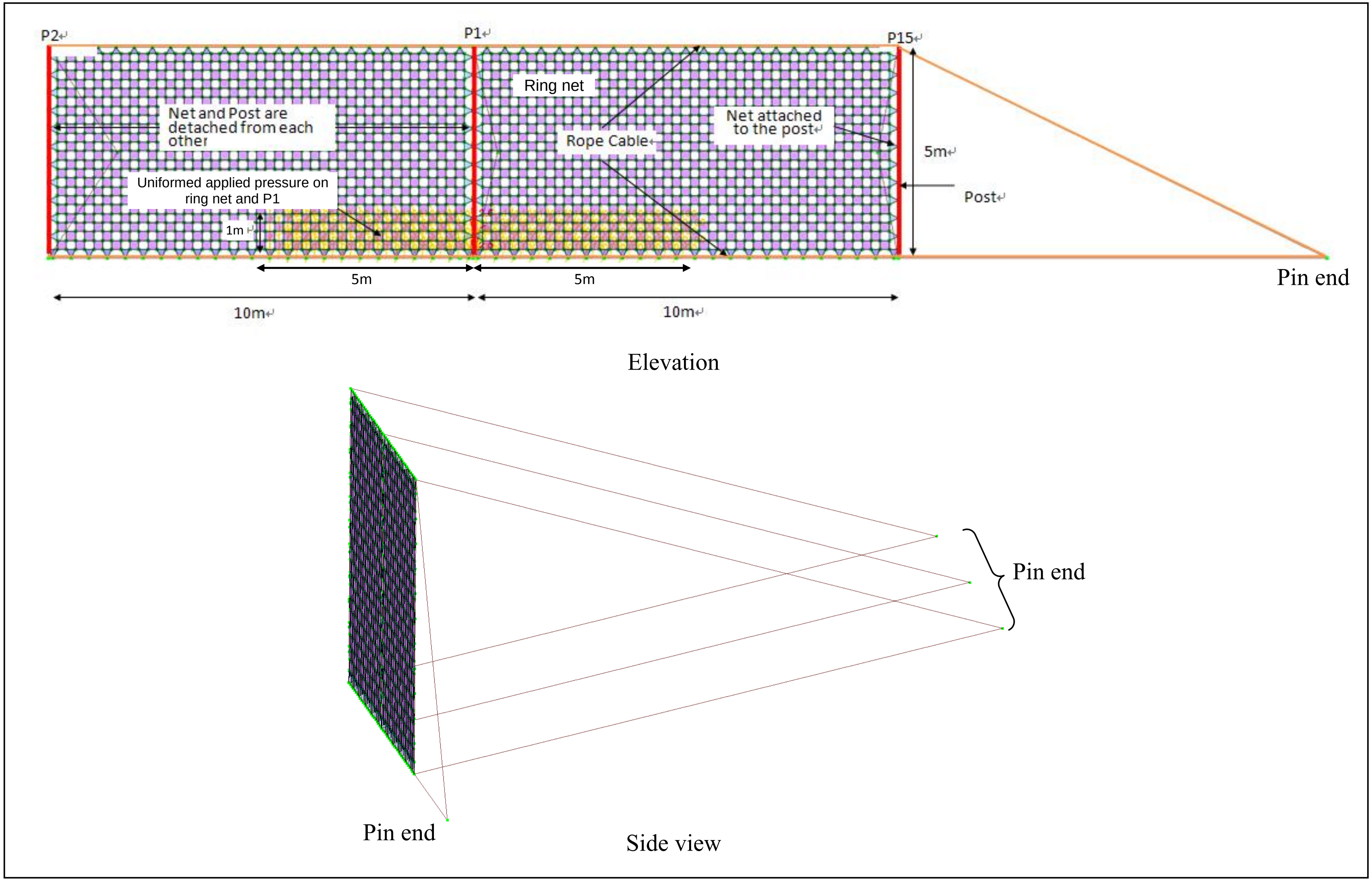

Figure B3 Set-up of the Numerical Model

Table of Contents Table of Contents Table of Contents Table of Contents

B.5 Back Analysis

Based on the back-analysis results of debris mobility, the estimated thickness of debris hitting the barrier is in the order of 1 m. The observed width of retained debris behind the barrier was about 10 m. Hence, impact debris thickness of 1 m and width of 10 m against the barrier were adopted in the analysis.

In the numerical analysis, the impact load is modelled as a uniformly distributed pseudo-static pressure. The magnitude of the uniformly distributed pressure (UDP) applied to the barrier is increased until a preset value is reached.

NIDA-MNN analysis indicates that the steel posts could have been subject to an axial load together with bending moments about both of the principal axes of the cross section. Failure of the posts can be determined using the plastic analysis recommended in the Code of Practice for Structural Uses of Steel, Hong Kong (BD, 2011). According to BD (2011), buckling failure of a column would take place when the section capacity factor (*R*) as defined in Equation B.1 is greater than unity (see Figure B4; i.e. when stress ratio (*R*) is greater than 1, it is considered that the column has buckled):

$$R = \frac{P}{P_{sq}} + \frac{M_x}{M_{CX}} + \frac{M_y}{M_{CY}} \quad \text{...} \quad \text{(B.1)}$$

where P = calculated axial force
M_X, M_Y = calculated bending moments about x- and y-axes
M_{CX}, M_{CY} = bending moment capacity about x- and y-axes
P_{sq} = squash load = σ_{yield} × sectional area
σ_{yield} = critical yield strength (174 MPa in this case history).

Also, shear failure can be checked by the following equation:

Shear failure of the posts has been checked if

$$V \,/\, V_c < 1 \text{ (i.e. no shear failure)} \quad \text{....................................} \quad \text{(B.2)}$$

where V = calculated shear stress
V_c = allowable shear stress.

Table of Contents Table of Contents Table of Contents Table of Contents

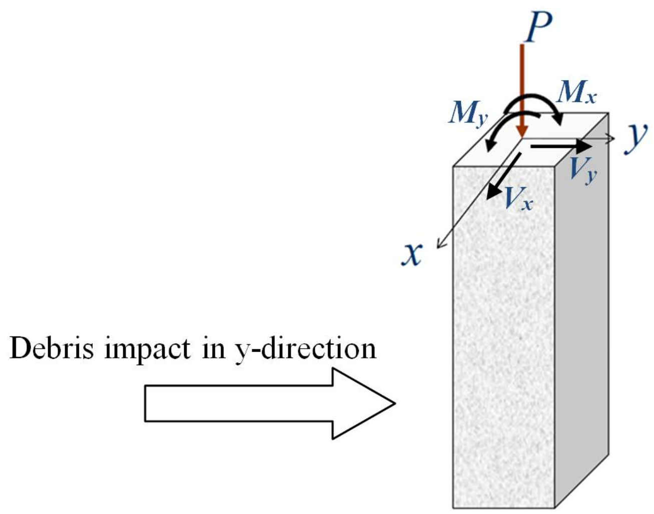

Figure B4 Schematic Diagram for Axial Load Plus Biaxial Moment for Slender Column

B.6 Results

Based on the site inspections, Posts P1 and P15 failed but not P2. The back analysis shows that both Posts P1 and P15 fail when the applied UDP is increased to 50 kPa. The large bending moment in P1 is induced by the UDP directly acting on the post, and the bending moment in P15 is induced by the lateral deformation of ring nets attached to the post. Failure of both P1 and P15 is due to the combined actions of bending moment and the axial compression load. The combined actions could have resulted in buckling failure of the posts. This may explain the reason for the failure of P15, which was not subject to direct hit by the landslide debris. The shear forces induced in the posts were found to be small and not critical.

The analysis also shows that the calculated maximum deformation of the ring net is about 2.5 m. The order of magnitude of the calculated deformation generally agrees with the site observation. The calculated results for P1, P2 and P15 are summarised in Table B1.

An attempt to estimate the upper limit of the applied UDP to cause an overall failure of the barrier has been made. It is noted that when the applied UDP is increased to 66 kPa, the tension developed in the lower rope cable reaches its ultimate tensile strength of 270 kN. The computed deformations of the flexible barrier panels and the calculated bending moment and shear force diagrams on the posts for an UDP of 50 kPa and 66 kPa respectively are shown in Figures B5 to B8.

In all the analyses, the calculated forces in Post P2 remained low. Structural assessments indicate that these calculated forces do not exceed the structural capacity of Post P2, which is consistent with the site observations.

Table of Contents
Table of Contents
Table of Contents
Table of Contents

Table B1 Summary of Calculated Results for Posts P1, P2 and P15

	UDP = 50 kPa							
	Values at the Maximum Combined Stress Ratio (see Equation B.1)				Maximum Values			
Post No.	Max. Stress Ratio (R)	P (kN)	M_x (kNm)	M_y (kNm)	V_x (kN)	V_y (kN)	Post Base Reaction in y-dir. (kN)	Cable Force (kN)
P2	***0.1***	21	0	0	0	0	47	227
P1	***1.0******	68	13.9	0.2	1.2	86.6	333	227
P15	***1.6******	92	4	20.4	15.6	3.4	51	227
	UDP = 66 kPa							
P2	***0.1***	25	0	0	0	0.1	62	***271***^
P1	***1.4******	83	19.8	0.1	1.6	123.3	438	***271***^
P15	***2.1******	107	5.5	26.6	20.7	4.8	67	***271***^

Notes:
(1) The calculated critical stress, σ_{cr} is 174 MPa and yield stress is 235 MPa for the designed post in this case (see Section B.5). As the calculated maximum shear force does not exceed the shear capacity of 263 kN for the post, shear failure of the post does not occur, which agrees with the site observations.
(2) The second order buckling equations presented in the Hong Kong code of practice for structural use of steel (BD, 2011) have also been used for carrying out the buckling analysis. It can be shown that the second order buckling equations provide similar results as shown above for the present case history.
(3) * Post fails in buckling. ^ Cable fails in tension.

Table of Contents
Table of Contents
Table of Contents
Table of Contents

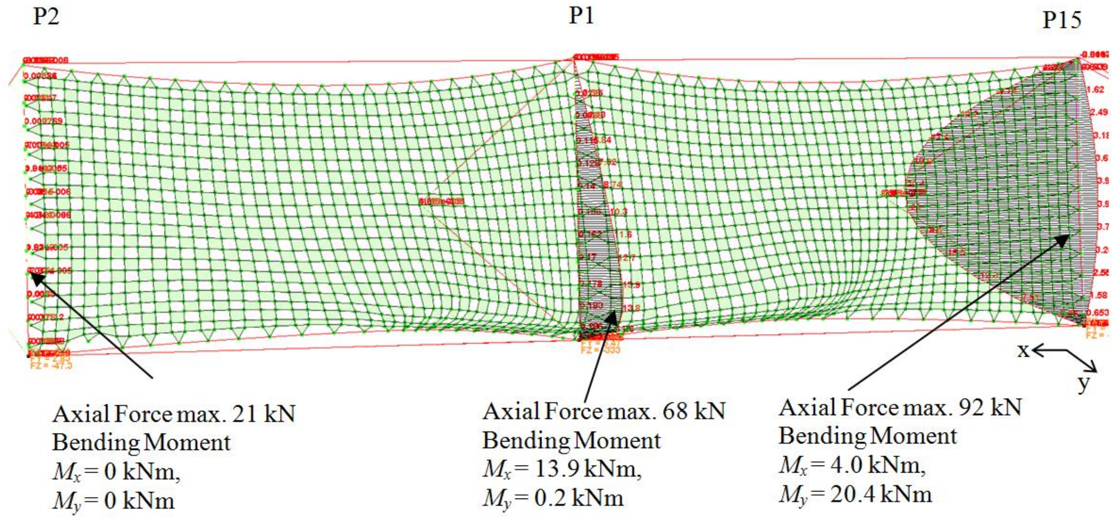

Figure B5 Bending Moment Diagrams of the Posts under UDP of 50 kPa

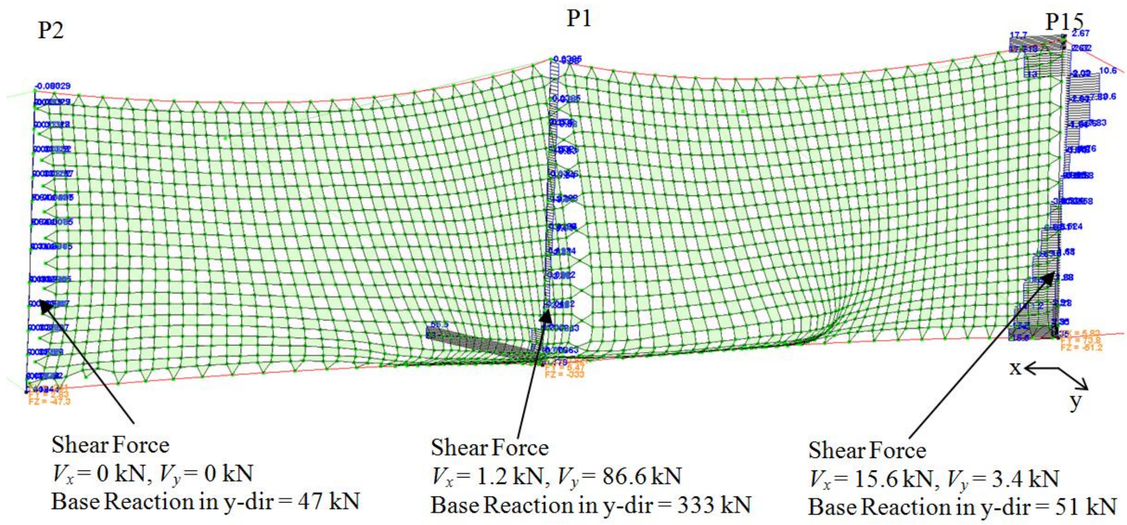

Figure B6 Shear Force Diagrams of the Posts under UDP of 50 kPa

Table of Contents
Table of Contents
Table of Contents
Table of Contents

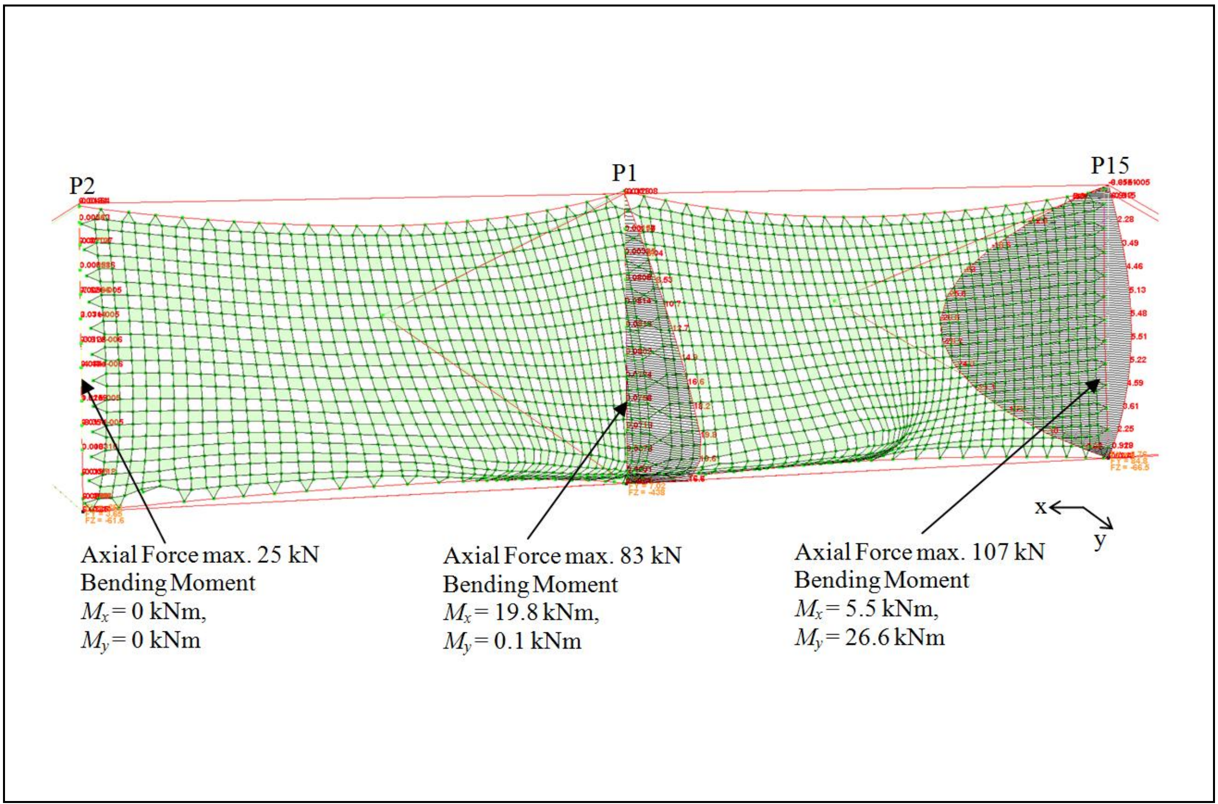

Figure B7 Bending Moment Diagrams of the Posts under UDP of 66 kPa

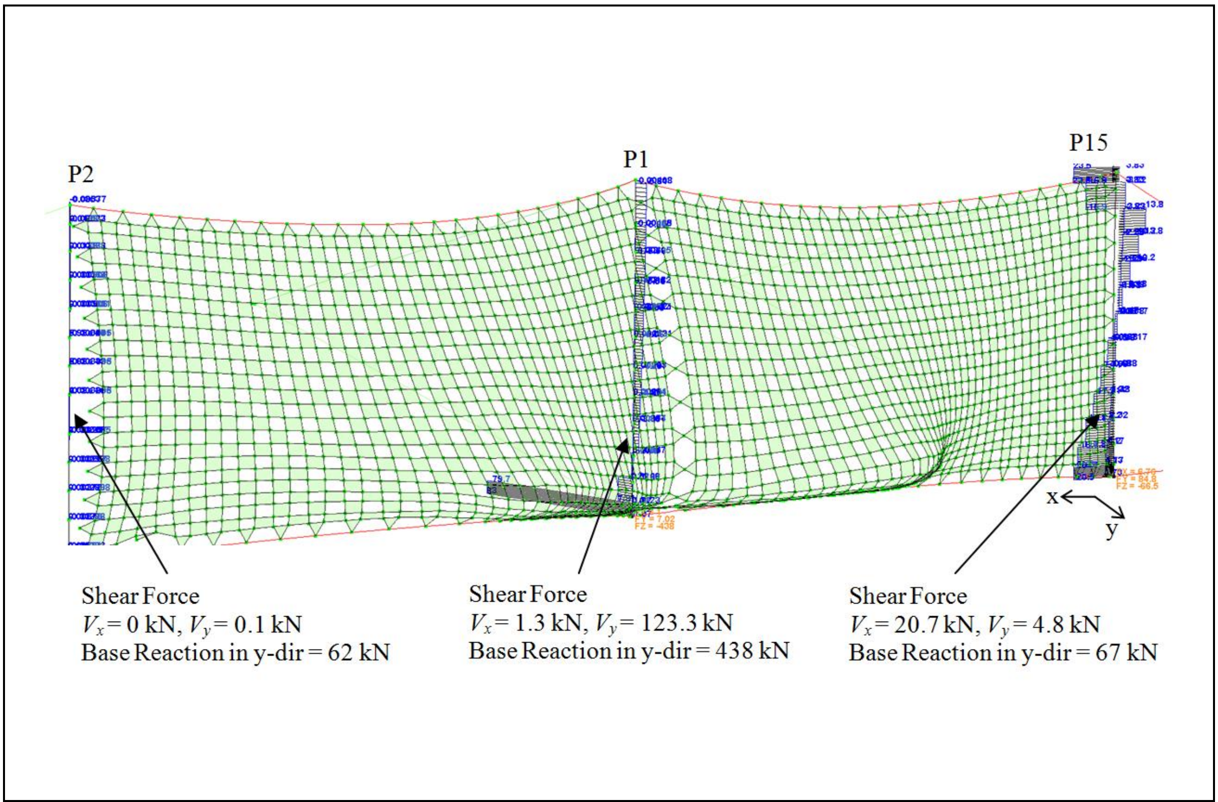

Figure B8 Shear Force Diagrams of the Posts under UDP of 66 kPa

Table of Contents
Table of Contents
Table of Contents
Table of Contents

The calculated base reaction in the debris impact direction at the foundation of Post P1 is 333 kN at UDP of 50 kPa, which is larger than the sliding resistance (R_s) of the shallow footing as estimated below:

Assumed soil friction angle,	$\phi' = 35°$	(for medium dense CDG, LMM (2004) refers)
Passive resistance,	$R_P = 0.5\, k_p\, \gamma H^2\, w$	(see Figure B9 for notations)
where	$k_p = 8$	(Geoguide 1, GEO (1994))
	$\gamma = 18$ kN/m^2	(assumed footing above the existing groundwater table)
	$H = 0.5$ m	(Height of footing)
	$w = 0.4$ m	(Width of footing)
Hence,	$R_P = 7$ kN	
Sliding resistance,	$R_S = N \tan \varphi'$	
where	$N = 68$ kN	(Axial compression force when UDP = 50 kPa, with self-weight and side friction neglected)
Hence,	$R_S = 48$ kN	

Total ultimate sliding resistance of the shallow footing = 7 + 48 = 55 kN < 333 kN.

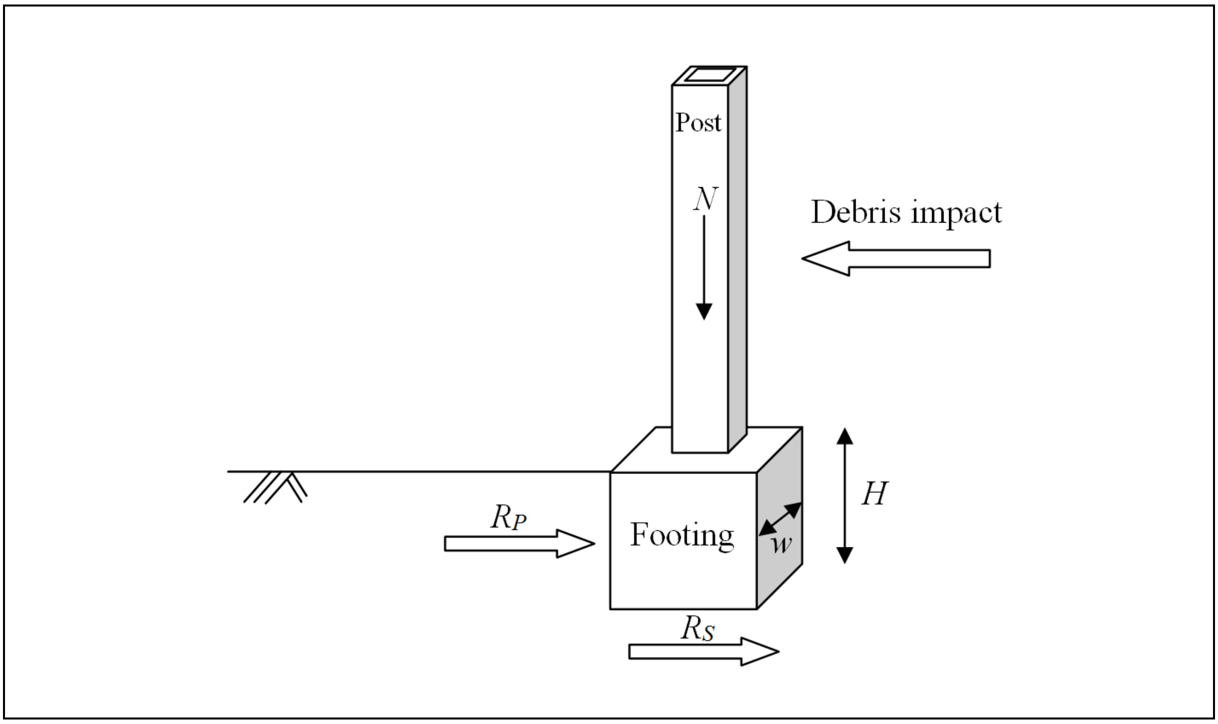

Figure B9 Schematic Drawing for Post and Footing

Table of Contents
Table of Contents
Table of Contents
Table of Contents

B.7 References

BD (2011). *Code of Practice for the Structural Use of Steel 2011*, Buildings Department, HKSAR Government, 388 p.

Chan, S.L., Zhou, Z.H. & Liu, Y.P. (2012). Numerical analysis and design of flexible barriers allowing for sliding nodes and large deflection effects. *Proceedings of the One Day Seminar on Natural Terrain Hazard Mitigation Measures 2012*, AGS(HK), Hong Kong, pp 29-43.

GEO (1994). *Geoguide 1 Guide to Retaining Design, 2nd Edition*. Geotechnical Engineering Office, Hong Kong, 268 p.

LMM (2004). *Design for Installation of Rockfall Barriers for Development at Choi Wan Road and Jordan Valley Kowloon*, LMM Consulting Engineers Ltd., 304 p.

Zhou, Z.H. & Chan S.L. (2011). *Nonlinear Finite Element Analysis and Design of Flexible Barrier*. Project Report, The Hong Kong Polytechnic University, 26 p.

Table of Contents
Table of Contents
Table of Contents
Table of Contents

GEO PUBLICATIONS AND ORDERING INFORMATION
土力工程處刊物及訂購資料

A selected list of major GEO publications is given in the next page. An up-to-date full list of GEO publications can be found at the CEDD Website http://www.cedd.gov.hk on the Internet under "Publications". Abstracts for the documents can also be found at the same website. Technical Guidance Notes are published on the CEDD Website from time to time to provide updates to GEO publications prior to their next revision.

部份土力工程處的主要刊物目錄刊載於下頁。而詳盡及最新的土力工程處刊物目錄，則登載於土木工程拓展署的互聯網網頁http://www.cedd.gov.hk 的"刊物"版面之內。刊物的摘要及更新刊物內容的工程技術指引，亦可在這個網址找到。

Copies of GEO publications (except geological maps and other publications which are free of charge) can be purchased either by:

Writing to
Publications Sales Unit,
Information Services Department,
Room 626, 6th Floor,
North Point Government Offices,
333 Java Road, North Point, Hong Kong.

or

- Calling the Publications Sales Section of Information Services Department (ISD) at (852) 2537 1910
- Visiting the online Government Bookstore at http:// www.bookstore.gov.hk
- Downloading the order form from the ISD website at http://www.isd.gov.hk and submitting the order online or by fax to (852) 2523 7195
- Placing order with ISD by e-mail at puborder@isd.gov.hk

讀者可採用以下方法購買土力工程處刊物(地質圖及免費刊物除外):

書面訂購
香港北角渣華道333號
北角政府合署6樓626室
政府新聞處
刊物銷售組

或

- 致電政府新聞處刊物銷售小組訂購 (電話：(852) 2537 1910)
- 進入網上「政府書店」選購，網址為 http://www.bookstore.gov.hk
- 透過政府新聞處的網站 (http://www.isd.gov.hk) 於網上遞交訂購表格，或將表格傳真至刊物銷售小組 (傳真：(852) 2523 7195)
- 以電郵方式訂購 (電郵地址：puborder@isd.gov.hk)

1:100 000, 1:20 000 and 1:5 000 geological maps can be purchased from:

Map Publications Centre/HK,
Survey & Mapping Office, Lands Department,
23th Floor, North Point Government Offices,
333 Java Road, North Point, Hong Kong.
Tel: (852) 2231 3187
Fax: (852) 2116 0774

讀者可於下列地點購買1:100 000、1:20 000及1:5 000地質圖：

香港北角渣華道333號
北角政府合署23樓
地政總署測繪處
電話: (852) 2231 3187
傳真: (852) 2116 0774

Requests for copies of Geological Survey Sheet Reports and other publications which are free of charge should be directed to:

For Geological Survey Sheet Reports which are free of charge:
Chief Geotechnical Engineer/Planning,
(Attn: Hong Kong Geological Survey Section)
Geotechnical Engineering Office,
Civil Engineering and Development Department,
Civil Engineering and Development Building,
101 Princess Margaret Road,
Homantin, Kowloon, Hong Kong.
Tel: (852) 2762 5380
Fax: (852) 2714 0247
E-mail: jsewell@cedd.gov.hk

For other publications which are free of charge:
Chief Geotechnical Engineer/Standards and Testing,
Geotechnical Engineering Office,
Civil Engineering and Development Department,
Civil Engineering and Development Building,
101 Princess Margaret Road,
Homantin, Kowloon, Hong Kong.
Tel: (852) 2762 5346
Fax: (852) 2714 0275
E-mail: florenceko@cedd.gov.hk

如欲索取地質調查報告及其他免費刊物，請致函：

免費地質調查報告:
香港九龍何文田公主道101號
土木工程拓展署大樓
土木工程拓展署
土力工程處
規劃部總土力工程師
(請交:香港地質調查組)
電話: (852) 2762 5380
傳真: (852) 2714 0247
電子郵件: jsewell@cedd.gov.hk

其他免費刊物:
香港九龍何文田公主道101號
土木工程拓展署大樓
土木工程拓展署
土力工程處
標準及測試部總土力工程師
電話: (852) 2762 5346
傳真: (852) 2714 0275
電子郵件: florenceko@cedd.gov.hk

Table of Contents
Table of Contents
Table of Contents
Table of Contents

MAJOR GEOTECHNICAL ENGINEERING OFFICE PUBLICATIONS
土力工程處之主要刊物

GEOTECHNICAL MANUALS

Geotechnical Manual for Slopes, 2nd Edition (1984), 302 p. (English Version), (Reprinted, 2011).

斜坡岩土工程手冊(1998)，308頁(1984年英文版的中文譯本)。

Highway Slope Manual (2000), 114 p.

GEOGUIDES

Geoguide 1	Guide to Retaining Wall Design, 2nd Edition (1993), 258 p. (Reprinted, 2007).
Geoguide 2	Guide to Site Investigation (1987), 359 p. (Reprinted, 2000).
Geoguide 3	Guide to Rock and Soil Descriptions (1988), 186 p. (Reprinted, 2000).
Geoguide 4	Guide to Cavern Engineering (1992), 148 p. (Reprinted, 1998).
Geoguide 5	Guide to Slope Maintenance, 3rd Edition (2003), 132 p. (English Version).
岩土指南第五冊	斜坡維修指南，第三版(2003)，120頁(中文版)。
Geoguide 6	Guide to Reinforced Fill Structure and Slope Design (2002), 236 p.
Geoguide 7	Guide to Soil Nail Design and Construction (2008), 97 p.

GEOSPECS

Geospec 1	Model Specification for Prestressed Ground Anchors, 2nd Edition (1989), 164 p. (Reprinted, 1997).
Geospec 3	Model Specification for Soil Testing (2001), 340 p.

GEO PUBLICATIONS

GCO Publication No. 1/90	Review of Design Methods for Excavations (1990), 187 p. (Reprinted, 2002).
GEO Publication No. 1/93	Review of Granular and Geotextile Filters (1993), 141 p.
GEO Publication No. 1/2006	Foundation Design and Construction (2006), 376 p.
GEO Publication No. 1/2007	Engineering Geological Practice in Hong Kong (2007), 278 p.
GEO Publication No. 1/2009	Prescriptive Measures for Man-Made Slopes and Retaining Walls (2009), 76 p.
GEO Publication No. 1/2011	Technical Guidelines on Landscape Treatment for Slopes (2011), 217 p.

GEOLOGICAL PUBLICATIONS

The Quaternary Geology of Hong Kong, by J.A. Fyfe, R. Shaw, S.D.G. Campbell, K.W. Lai & P.A. Kirk (2000), 210 p. plus 6 maps.

The Pre-Quaternary Geology of Hong Kong, by R.J. Sewell, S.D.G. Campbell, C.J.N. Fletcher, K.W. Lai & P.A. Kirk (2000), 181 p. plus 4 maps.

TECHNICAL GUIDANCE NOTES

TGN 1	Technical Guidance Documents